ECOLOGICAL MODELLING 196 (2006) 289–312

available at www.sciencedirect.com

SCIENCE DIRECT®

journal homepage: www.elsevier.com/locate/ecolmodel

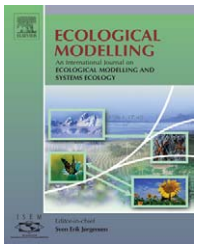

Intercomparison of techniques to model water stress effects on CO_2 and energy exchange in temperate and boreal deciduous forests

R.F. Grant[a,*], Y. Zhang[b], F. Yuan[c], S. Wang[b], P.J. Hanson[d], D. Gaumont-Guay[e], J. Chen[f], T.A. Black[e], A. Barr[g], D.D. Baldocchi[h], A. Arain[c]

[a] Department of Renewable Resources, University of Alberta, Edmonton, Alta., Canada T6G 2E3
[b] Canadian Centre for Remote Sensing, Ottawa, Ont., Canada
[c] School of Geography and Geology, McMaster University, Hamilton, Ont., Canada
[d] Environmental Sciences Division, Oak Ridge National Laboratory, Oak Ridge, TN, USA
[e] Department of Soil Science, University of British Columbia, Vancouver, BC, Canada
[f] Department of Geography, University of Toronto, Toronto, Ont., Canada
[g] Environment Canada, Saskatoon, Sask., Canada
[h] Department of Environmental Science, Policy, & Management, University of California-Berkeley, Berkeley, CA, USA

ARTICLE INFO

Article history:
Received 26 May 2005
Received in revised form 9 December 2005
Accepted 9 February 2006
Published on line 3 April 2006

Keywords:
Water stress
CO_2 exchange
Energy exchange
Ecosystem modeling
Deciduous forests
Net primary productivity
Net ecosystem productivity

ABSTRACT

Soil water deficits are a key controller of net ecosystem productivity (NEP) in deciduous broadleaf forests. Mathematical models of forest NEP need to represent the processes by which this control is exerted if they are to be used to predict the impacts of changing hydrology on forest C stocks. The key processes controlling NEP during soil water deficits are hydraulic limitations to water transfer in soil, roots, stems and leaves that impose constraints on gross primary productivity (GPP). We compare five ecosystem models with different techniques to simulate these processes for their ability to model reduced latent versus sensible heat fluxes, earlier diurnal declines in CO_2 influxes and reduced soil CO_2 effluxes during soil drying. Model accuracy was assessed using energy and CO_2 fluxes measured by eddy covariance and surface chambers in a warm temperate and a cool boreal deciduous forest during a drying period. Diurnal declines in CO_2 influxes during soil drying were consistently simulated by models in which soil drying lowered root and canopy water potentials (ψ_c) and raised soil and root hydraulic resistances. Leaf stomatal conductance (g_l), derived in these models from non-linear functions of ψ_c, then became more sensitive to diurnal changes in vapor pressure deficits (D). Diurnal declines in CO_2 influxes could be simulated with comparable accuracy under most conditions by a model in which g_l was empirically related to soil water potential and D, although these declines were sometimes not fully simulated. CO_2 influxes declined too rapidly with diurnal rises in D in another model in which g_l was calculated from CO_2 fixation which was empirically related to soil water content. Divergences in modeled versus measured half-hourly or hourly CO_2 exchange were also apparent in modeled versus measured annual GPP, net primary productivity (NPP) and NEP. The ability to distinguish among alternative algorithms

* *Corresponding author*. Tel.: +1 403 492 4413; fax: +1 780 492 1767.
E-mail address: robert.grant@afhe.ualberta.ca (R.F. Grant).
0304-3800/$ – see front matter
doi:10.1016/j.ecolmodel.2006.02.035

for their accuracy in calculating CO_2 and energy fluxes was often limited by uncertainty in the measurement of these fluxes using eddy covariance, especially when low wind speeds and stable boundary layers reduced atmospheric turbulence.

1. Introduction

Water availability has been estimated to control net primary productivity (NPP) to some extent in 64% of deciduous broadleaf forest area (Churkina and Running, 1998). Some climate change scenarios indicate an increase in the frequency and severity of droughts that may alter the distribution and NPP of tree species in deciduous forests (Pastor and Post, 1988). The impact of droughts on deciduous forest NPP depends upon mechanisms of drought avoidance and tolerance, including stomatal closure, deep rooting and osmotic adjustment. Projections of these impacts on NPP are frequently made with ecosystem models in which these mechanisms are represented at varying levels of detail. However, Hanson et al. (2004) found that the predictive ability of a diverse range of these models deteriorated under drought conditions, suggesting that further work is needed to evaluate and improve ecosystem model performance when water is limiting.

There are different views on the mechanisms by which soil water deficits limit NPP. Schulze (1993) hypothesized that abscisic acid (ABA), produced by drying root tips and transported through the xylem, caused leaf stomatal conductance (g_l) and hence CO_2 fixation to decline. This hypothesis was developed from earlier work by Gollan et al. (1986) who found that declines in g_l occurred independently of leaf water potential (ψ_l). However Tardieu and Davies (1993) found that sensitivity of g_l to ABA depended on ψ_l, so that both ABA and ψ_l were required to model g_l robustly as part of a general scheme for soil–plant–atmosphere water relations.

There are two stages to modeling such a general scheme: (1) solving for canopy stomatal conductance (g_c) from plant water status as determined by soil and atmospheric water status, and (2) calculating the impact of declines in g_c on CO_2 fixation. The first stage requires the coupling of canopy transpiration, as affected by atmospheric water status, with root water uptake, as affected by soil water status. Transpiration is most commonly calculated from formulations of the Penman–Monteith equation (Monteith, 1965) at daily (Chen et al., 1999; Grote et al., 1998; Hunt et al., 1999; Kimball et al., 1997; Landsberg and Waring, 1997; Potter, 1997; Wullschleger et al., 2003) or hourly (Wang and Jarvis, 1990; Williams et al., 1996) time steps, or from a first-order closure of the canopy energy balance at 1/2 or 1 hour time steps (Amthor et al., 1994; Baldocchi and Wilson, 2001; Grant, 2001; King et al., 1997; Nikolov, 1997; Wang et al., 2002a,b). In earlier model intercomparisons, Hanson et al. (2004) found that models that used a complete energy balance were best able to simulate mass and energy exchange over a temperate deciduous forest. The net radiation and aerodynamic terms in these calculations require canopy LAI which may be modeled from leaf mass (Amthor et al., 1994; Grant, 2001; Wang et al., 2002a,b; Wullschleger et al., 2003) or prescribed from site measurements (Baldocchi and Wilson, 2001; King et al., 1997; Hunt et al., 1999; Wang and Jarvis, 1990; Williams et al., 1996).

The formulation of g_c from root and/or canopy water status for use in calculating transpiration appears to be the most critical process causing differences in predicted fluxes of carbon and water among ecosystem models (Kramer et al., 2002). Values of g_c are sometimes calculated from empirical functions of photosynthetically active radiation (PAR), air temperature (T_a), vapor pressure deficit (D) and soil water potential (ψ_s) (Amthor et al., 1994; Chen et al., 1999; Wullschleger et al., 2003), and also of atmospheric CO_2 concentration (C_a) (Hunt et al., 1999; Kimball et al., 1997). These functions avoid the calculation of canopy water status, driving g_c directly from soil and atmospheric water status as proposed by Kramer (1993). Stomatal conductance is more commonly calculated from a Ball–Woodrow–Berry function driven by atmospheric humidity or D (Ball, 1988; Ball et al., 1987), CO_2 fixation and C_a (Baldocchi and Wilson, 2001; King et al., 1997; Nikolov, 1997; Wang and Jarvis, 1990; Wang et al., 2002a,b). This function does not represent either an ABA or a hydraulic effect on g_c during soil water deficits, and so requires re-parameterization with changing ψ_s (Reichstein et al., 2002) or soil water content (θ) (Wang and Leuning, 1998; Arain et al., 2002). Stomatal conductance is also calculated directly from CO_2 fixation divided by atmospheric – intercellular CO_2 concentration differences ($C_a - C_i$), coupled to non-linear functions of canopy water potential (ψ_c) (Tuzet et al., 2003) or turgor potential (ψ_t) (Grant, 2001), thereby avoiding an empirical association with humidity. These models do not simulate a direct effect of root water status on g_c. However soil drying in these models causes soil and root hydraulic resistances to increase and so causes ψ_c to decline more rapidly with rise in transpiration. Therefore g_c becomes more sensitive to soil and root water status as ψ_s declines. Calculations of g_c from Ball–Woodrow–Berry functions or from ($C_a - C_i$) and ψ_c are driven by CO_2 fixation, usually calculated from Farquhar et al. (1980), through which effects of PAR, T_a and C_a on g_c are mediated. Alternatively, Williams et al. (1996) calculated a value for g_c that meets criteria for maximizing CO_2 fixation while avoiding low ψ_c.

The modeling of root water uptake with which canopy transpiration is coupled is much less developed than is that of canopy transpiration, and in some models it is omitted (Baldocchi and Wilson, 2001; Wang and Jarvis, 1990). In other models, g_s is an empirical function of ψ_s as described earlier, so that ψ_s may directly limit transpiration and hence root water uptake. Potential root water uptake is sometimes calculated from normalized θ and from fine root mass and hydraulic conductivity, and used to limit canopy transpiration (Grote et al., 1998). These models cannot account for the influence of ψ_c on spatial and temporal patterns of root water uptake. The most detailed models calculate uptake from water potentials and hydraulic resistances along a soil–root–canopy pathway from single (Tuzet et al., 2003; Williams et al., 1996) or multiple (Grant, 2001; Wang et al., 2002a,b) soil layers to single (Grant, 2001; Tuzet et al., 2003; Wang et al., 2002a,b) or multiple (Williams et al., 1996) canopy layers. These resistances

have been found necessary to the modeling of seasonal precipitation effects on mass and energy exchange (Williams et al., 1998). Root water uptake in these models is equilibrated with canopy transpiration and capacitance through a solution for ψ_c (Grant, 2001; Wang et al., 2002a,b) or g_s (Williams et al., 1996). Modeled ψ_c may also be used with canopy osmotic potential (ψ_π) to simulate osmotic adjustment effects on ψ_t from which water deficit effects on g_l are calculated (Grant, 2001). Certain models (e.g. Nikolov, 1997) attempt to represent chemical (ABA) as well as hydraulic signals from roots to stomates as proposed by Tardieu and Davies (1993), but quantitative hypotheses for these signals are not yet well developed. Although hydraulic models are most likely to capture ψ_s effects on diurnal CO_2 and energy exchange, tests of these models have been limited, or have not been performed (e.g. Tuzet et al., 2003), indicating a need for well-constrained testing against field measurements.

The second stage in modeling soil–plant–atmosphere water relations, the impact of g_c on CO_2 fixation, is poorly developed. In some models, the calculation of canopy water status is avoided so that NPP is directly affected by soil and/or atmospheric water status. Landsberg and Waring (1997) calculate NPP from absorbed PAR multiplied by the minimum of scaling factors for soil or atmospheric water deficits, so that interactions between soil and atmospheric water deficits on NPP are not modeled. When g_s is modeled from Ball–Woodrow–Berry functions, water deficit effects are sometimes assumed to be non-stomatal (i.e. mesophyll, acting directly on CO_2 fixation) so that CO_2 fixation is multiplied by scaling factors calculated from ψ_c (Wang et al., 2002a,b). In other models, water deficit effects on CO_2 fixation are assumed to be entirely stomatal (Williams et al., 1996), or both stomatal and non-stomatal (Grant, 2001; Arain et al., 2002) so that CO_2 fixation arises from a solution for intercellular CO_2 concentration (C_i) at which diffusive and biochemical CO_2 fluxes are equal. These models can simulate interactions between soil and atmospheric water deficits on CO_2 fixation.

The modeling of water deficit effects on NEP also requires the modeling of those on autotrophic (R_a) and heterotrophic (R_h) respiration. R_a is usually assumed not to be directly affected by root or canopy water status, but is indirectly affected through changes in CO_2 fixation and consequent phytomass growth caused by changes in root or canopy water status. R_h in most models declines with relative water-filled pore space (RWFPS = θ/θ_{sat}) below its value at field capacity, based on laboratory observations of soil CO_2 emissions versus θ (e.g. Bunnell et al., 1977; Orchard and Cook, 1983).

Model estimates of water deficit effects on net ecosystem CO_2 exchange can be calculated from CO_2 fixation—$R_a - R_h$ and compared with measurements of CO_2 exchange during soil drying using eddy covariance. However the different modeling hypotheses described above have been subjected to only limited comparative testing against measurements of mass and energy exchange in deciduous forests, particularly during soil drying (e.g. Hanson et al., 2004). In this paper, we analyze the ability of five models participating in the Fluxnet-Canada Research Network (FRCN) to simulate mass and energy exchange during different water stress events in terms of the hypotheses for water stress on which each model is based. These models used different approaches to simulate soil–plant–atmosphere water relations. In some models, g_c was calculated from ψ_c by coupling transpiration with hydraulic schemes for root water uptake, while in others g_c was calculated directly from θ or from CO_2 fixation constrained by θ. CO_2 fixation was constrained in some models only by stomatal effects through g_l, in other models by non-stomatal effects driven by ψ_c, and in others by both stomatal and non-stomatal effects.

This analysis is intended to establish the comparative merits of different modeling hypotheses for water stress and to seek consensus on further development of these hypotheses. The two test sites selected for this analysis are in different climatic zones (temperate and boreal), but both experience water stress events that are predicted to become more severe under some climate change scenarios. This model intercomparison builds upon an earlier one in which we examined the comparative merits of different modeling hypotheses for high temperature stress in conifers as a part of the Fluxnet-Canada Research Network (FCRN) (Grant et al., 2005).

2. Model descriptions

The five models included in the FCRN all function at time steps of 1 h or less, and so represent the higher end of the range of temporal resolution included in earlier model intercomparisons (e.g. Amthor et al., 2001; Hanson et al., 2004). Although these models were developed for the common purpose of simulating terrestrial net ecosystem productivity (NEP), differences have emerged in key algorithms and parameters for soil and climate effects on soil–plant–atmosphere mass and energy exchange. The key algorithms and parameters for these effects in each of the five models are described in our earlier publication in this journal (Grant et al., 2005). A brief introduction to each model is given below with reference to model equations (e.g. A.x.x) in the Appendix of this earlier publication.

2.1. *Boreal ecosystem productivity simulator (BEPS)*

BEPS (Liu et al., 1997; Chen et al., 1999) was developed at the Canadian Centre for Remote Sensing (CCRS) and the University of Toronto for short-term carbon cycle simulations, while the Integrated Terrestrial Ecosystem Carbon Cycle Model (InTEC) (Chen et al., 2000a,b), used here for spin-up of soil carbon, was developed for long-term carbon cycle simulations. These models have been used with remotely sensed estimates of leaf area index (LAI) and land cover, and with Soil Landscapes of Canada (SLC), forest inventory and gridded meteorological data to make regional and national estimates of NPP, NEP and net biome productivity (NBP) (Chen et al., 2003).

CO_2 fixation in BEPS was constrained by leaf stomatal conductance (g_l) (A.1.4) calculated empirically from canopy temperature T_c (Humphreys et al., 2003), θ (Bonan, 1991; Zierl, 2001), humidity (Dang et al., 1997) and global radiation based on Jarvis (1976) (A.2.1). Values of g_l were aggregated to g_c from weighted averages of sunlit and shaded leaf area for vegetation layers (A.2.3). Transpiration was calculated from g_c using the Penman–Monteith equation (A.6.1). Water uptake from each

soil layer was calculated as a fraction of transpiration weighted by root fraction and ψ_s (A.6.6).

2.2. Ecosys

Ecosys (http://www.ecosys.rr.ualberta.ca/; Grant, 2001) was developed at the University of Alberta as a detailed, comprehensive model of terrestrial ecosystems. This model provides a means to anticipate ecosystem behavior under different environmental conditions (soils, climates and managements). Ecosys is used to estimate the impacts of climate, land use practices and soil management on primary productivity, soil and atmospheric quality and associated resource requirements (e.g. water, fertilizer) of diverse terrestrial ecosystems (e.g. Grant, 2003; Grant et al., 2001, 2003).

Water deficits in ecosys constrain CO_2 fixation through g_l and non-stomatal effects. Values of g_l and g_c were calculated from a two-stage convergence solution for the transfer of water and heat through the soil–root–canopy system. The first stage of this solution required convergence to T_c at which the first-order closure of the canopy energy balance was achieved. The second state required convergence to ψ_c at which the difference between canopy transpiration E_c from the energy balance (A.6.1) and total water uptake U_r from all rooted layers in the soil (A.6.6) equalled the difference between canopy water content at ψ_c from the previous hour and that from the current hour to account for plant capacitance. Values of ψ_c and g_l were then used in a convergence solution for C_i of each leaf at which the diffusion rate of gaseous CO_2 between C_a and C_i through g_l equalled the carboxylation rate at the aqueous equivalent of C_i (A.1.13).

2.3. Canadian Land Surface Scheme (CLASS) biospheric components (C-CLASSa and C-CLASSm)

CLASS (Verseghy, 2000) was developed by the Meteorological Service of Canada (MSC) for coupling with the Canadian General Circulation Model (CGCM) in regional climate–ecosystem interactions. CLASS has participated in the International Project for Intercomparison of Land–Surface Parameterization Schemes (PILPS). Versions of the CLASS biospheric component (C-CLASS) are being developed at McMaster University (C-CLASSm) (Arain et al., 2002; Kothavala et al., 2005) and the University of Alberta (C-CLASSa) (Wang et al., 2001, 2002a,b; Zhang et al., 2004).

In C-CLASSa, soil water deficits effects constrained CO_2 fixation (A.1.4) and hence g_c (A.2.1) through ψ_c at which plant transpiration from a first-order closure of the canopy energy balance (A.6.1) equilibrated with root water uptake along a soil–root–canopy ψ gradient (A.6.6) (Wang et al., 2002b). In C-CLASSm, CO_2 fixation was constrained directly by θ (A.1.4), and then used to calculate g_c from Ball et al. (1987) (A.2.1). CO_2 fixation, g_c and C_i, were then solved iteratively until energy balance closure was achieved.

2.4. Ecological Assimilation of Climate and Land Observations (EALCO)

EALCO was developed at the Canadian Centre for Remote Sensing to study ecosystem–climate interactions by assimilating Earth Observation datasets (both in situ and satellite) (Wang et al., 2002c). EALCO algorithms for soil water deficit effects on soil–plant–atmosphere water transfer and ψ_c were shared with C-CLASSa (Wang et al., 2002b). However EALCO used a different algorithm from C-CLASSa for the effects of ψ_c on CO_2 fixation (A.1.4).

3. Modeling experiment

3.1. Experimental sites

3.1.1. Walker Branch Watershed

The Walker Branch Watershed (WB) (35°57′N; 84°17′W; 250–330 m elevation) in 1998 was a 50–80-year-old largely upland temperate oak forest, located on typic Paleudults in the U.S. Department of Energy's National Environmental Research Park near Oak Ridge, TN. It is representative of much of the eastern deciduous hardwood forests that occupy ~617,000 km^2 or 42% of the total forested area in the Eastern United States. Site and soil data are given in Table 1. Eddy covariance (EC) techniques used to measure mass and energy exchange are described in Wilson et al. (2001a,b) and Baldocchi et al. (2001). Gaps in CO_2 flux data caused by unfavorable site conditions ($u^* < 0.175\ m\ s^{-1}$) or instrument failure were filled by a non-linear regression method based on relationships of daytime fluxes with radiation and temperature, and of nighttime fluxes with temperature. These relationships were parameterized from measurements under favorable site conditions during six bimonthly periods (Falge et al., 2001).

3.1.2. Southern Old Aspen

The Southern Old Aspen (SOA) site in 2002 was a 75-year-old aspen forest, located on a typic Haploboroll overlying a glacial till in Prince Albert National Park, Sask., Canada (53.6°N, 106.2°W) near the southern limit of the boreal forest. Comparable aspen stands occupy 10–20% of the southern boreal forest. Site and soil data are given in Table 2. EC techniques used to measure mass and energy exchange are described in Blanken et al. (2001) and Griffis et al. (2003). Gap filling techniques to replace rejected eddy covariance CO_2 fluxes were described in Barr et al. (2002).

3.2. Model runs

Each model was provided with hourly (WB 1993–2000) or half-hourly (SOA 1994–2002) meteorological data (shortwave radiation, longwave radiation (for the C-CLASS models), T_a, relative humidity, wind speed and precipitation) recorded at each flux tower, and with the site and soil properties in Tables 1 and 2. Each model used its own algorithms and parameters for plant and soil biological processes, key values of which are given in the Appendix of Grant et al. (2005). Observed dates were used to guide model algorithms for timing of leafout and leaf fall. Model-specific protocols were followed for initialization and spin-up, although all models were run for at least 5 years at WB (1993–1997) or 8 years at SOA (1994–2001) under site conditions before comparison with measured val-

Table 1 – Site and soil characteristics of the Walker Branch Watershed

Site characteristics

Latitude: 35°57′N
Longitude: 84°17′W
Elevation: 250–330 m
Mean annual precipitation: 1358 mm
Mean annual temperature: 14.2 °C
Dominant vegetation 60-year-old oak *Quercus alba*, *Quercus prinus* and *Acer rubrum*
Understory vegetation *A. rubrum*, *Cornus Florida*
Mean basal area (1999): 22.8 m^2 ha^{-1} (overstory) 5.6 m^2 ha^{-1} (understory)

Soil characteristics[a]

Horizon	A	E	AB	B1	B21t	B22t
Depth to bottom (m)	0.07	0.33	0.43	0.51	0.71	1.07
Bulk density (Mg m^{-3})	1.06	1.27	1.43	1.31	1.29	1.2
Field capacity (m^3 m^{-3})	0.28	0.27	0.27	0.29	0.38	0.38
Wilting point (m^3 m^{-3})	0.09	0.10	0.09	0.12	0.22	0.22
K_{sat} (mm h^{-1})	39.7	23.5	34.8	10.7	2.8	2.8
Sand (g kg^{-1})	340	280	280	240	130	130
Silt (g kg^{-1})	630	600	640	560	430	360
Clay (g kg^{-1})	30	120	80	200	400	510
Coarse fragments (m^3 m^{-3})	0.14	0.14	0.17	0.17	0.17	0.17
pH	4.5	4.2	4.4	4.2	4.2	4.2
CEC ($cmol^{(+)}$ kg^{-1})	5.64	1.94	2.08	2.73	5.42	8.92
Organic C (g kg^{-1})	36.0	9.6	3.6	3.4	3.5	3.4
Total N (g Mg^{-1})	1580	500	310	310	410	390
Total P (g Mg^{-1})	200	200	100	200	100	200

[a] Peters et al. (1970).

Table 2 – Site and soil characteristics of the Southern Old Aspen site

Site characteristics

Latitude: 53.6°N
Longitude: 106.2°W
Elevation: 600 m
Mean annual precipitation: 484 mm
Mean annual temperature: 1.5 °C
Dominant vegetation: 80-year-old aspen (*Populus tremuloides*)
Understory vegetation: hazelnut (*Corylus cornuta*)
Mean basal area (1994) 33.5 m^2 ha^{-1} (overstory)

Soil characteristics[a]

Horizon	L	F	H	Ae	Bt	Bmk	Ck1	Ck2
Depth to bottom (m)	0.02	0.05	0.10	0.32	0.70	0.85	1.25	1.85
Bulk density (Mg m^{-3})	0.09	0.11	0.19	1.38	1.53	1.67	1.67	1.67
Field capacity (m^3 m^{-3})	0.62[b]	0.62	0.71	0.17	0.23	0.19	0.18	0.21
Wilting point (m^3 m^{-3})	0.15[b]	0.15	0.22	0.07	0.13	0.11	0.10	0.13
K_{sat} (mm h^{-1})	7.2	7.2	7.2	20.2	5.3	5.5	5.2	5.2
Sand (g kg^{-1})	–	–	–	589	568	485	484	484
Silt (g kg^{-1})	–	–	–	293	187	280	276	276
Clay (g kg^{-1})	–	–	–	118	245	235	240	240
Coarse fragments (m^3 m^{-3})	0	0	0	0	0	0	0	0
pH	6.4	6.5	6.6	6.6	6.5	6.8	8.5	8.5
CEC ($cmol^{(+)}$ kg^{-1})	103	119	120	9.2	14	12	12	10
Organic C (g kg^{-1})	430	415	313	6.2	3.4	2.0	3.4	3.4
Total N (g Mg^{-1})	20199	21573	19522	521	317	286	200	200
Total P (g Mg^{-1})	1442	1269	1220	212	304	459	448	448

[a] Anderson (1998).
[b] LFH values estimated from Letts et al. (2000).

ues to avoid sensitivity of model output to model initialization.

Model performance was evaluated during soil drying using parameters (intercepts, slopes) from regressions of modeled on measured fluxes (allowing overestimates or underestimates of measured values to be inferred from intercepts >0 or <0 and from slopes >1 or <1, respectively), and using statistics (coefficients of determination and root mean squares of difference) from regressions of measured on modeled fluxes (allowing differences between modeled and measured fluxes to be expressed in terms of the same measured values). These regressions were conducted with hourly-averaged fluxes and with daily total fluxes during periods of contrasting θ. Model-specific protocols are described in more detail below.

3.2.1. *BEPS*

The stand ages (Tables 1 and 2) were used to spin-up the soil carbon pool using InTEC. Soil water content at the beginning of the modeling period was derived from spin-up model runs using BEPS for 8 years at WB and for 7 years at SOA. LAI and clumping index of the overstory were set to 5.8 and 0.8, respectively, at WB, and to 3.3 and 0.9, respectively, at SOA, based on site observations. The understory LAI was set at 3.0 and 2.3 at WB and SOA, respectively.

3.2.2. *Ecosys*

Ecosys was initialized at seeding on soil with the properties given in Tables 1 and 2, and with above- and below-ground residue corresponding to that left after logging. Ecosys was then run for 60 (WB) or 80 (SOA) years under repeated sequences of meteorological data from each site before comparison with measurements. At the end of these runs, plant C stocks had attained values similar to those recorded at each site. Plant parameters used in these runs were those for warm temperate (WB) and boreal (SOA) deciduous functional types which differed only in their temperature functions (A.1.2, A.3.3, A.4.2, A.5.11). A boreal deciduous understory was added to the run at SOA because the hazelnut understory at this site was particularly productive (Black et al., 1996). Two additional soil layers were modeled below the lowest layer in Tables 1 and 2 so that water fluxes modeled in the rooting zone were largely independent of assumptions about the lower boundary.

3.2.3. *C-CLASSa*

C-CLASSa was initialized at seeding on soil with the properties given in Tables 1 and 2, and with above- and below-ground residue corresponding to that left after logging. C-CLASSa was then run for 60 (WB) or 80 (SOA) years under repeated sequences of meteorological data from each site before comparison with measurements. Plant parameters used in these runs were those for warm temperate (WB) and boreal (SOA) deciduous functional types which differed only in their temperature functions (A.1.2, A.3.3, A.4.2, A.5.11). Root distribution was fixed in the model runs because environmental conditions simulated in the third soil layer could not accurately represent those in the root zone due to the coarse spatial resolution in the model (A.6.7). T_s and θ of the lower soil boundary (depth = 4.1 m) were held constant during the model run.

3.2.4. *C-CLASSm*

Initial C pools (sapwood, coarse and fine root, litter and soil layer (A.6.7)) and soil physical and chemical properties were assigned from site-specific measurements given in Tables 1 and 2. The active root zone was assumed to be the second soil layer (A.4.3). Rooting depths were set to 0.8 m at WB and 0.6 m at SOA. The default CLASS root density function (an exponential decrease with depth) was used for root distribution in the three model layers (A.6.7). Model simulations were run for 1 year at WB and 6 years at SOA using observed half-hourly weather data for 2000 and 2002, respectively. Minimum and maximum LAI were set to 6.0 and 6.9, respectively, at WB, and to 2.0 at SOA. Model spin-up was not performed because the model was initialized from observations.

3.2.5. *EALCO*

EALCO was initialized with pool sizes estimated from site observations (Tables 1 and 2). LAI was simulated from leaf C but was constrained by the observed maximum leaf area index. The model was run with observed weather data from 1993 to 2000 at WB and from 2000 to 2002 at SOA. Root distribution was initialized by allocating half of the total fine root to the top 0.35 m and the remainder to the next 1.15 m. No water flux across the soil lower boundary was assumed.

4. Results

4.1. *Soil water deficits*

4.1.1. *Walker branch*

Low precipitation during the summer of 1998 (Fig. 1a) caused θ measured in the upper 0.35 m to decline from near field capacity (Table 1) in mid-June to below wilting point in early September Fig. 1b). This decline was fully simulated by models that accounted for the effects of coarse fragments (Table 1) on soil water retention (ecosys and C-CLASSa). The decline in θ was underestimated by other models in which this effect was ignored (BEPS and C-CLASSm). This underestimation was not likely caused by underestimated evapotranspiration (A.6.1) (Fig. 1b), although total ET in BEPS was lower than those in the other models, but more likely by differences in the allocation of water uptake among soil layers. Allocation in BEPS and C-CLASSm was calculated from empirical relationships with root depth distributions while allocation in the other models was calculated from hydraulic potentials and resistances along soil–root–canopy pathways in each soil layer (A.6.6). Values of θ were overestimated by EALCO, although the magnitude of the decline in θ was otherwise well simulated.

4.1.2. *Southern Old Aspen*

Following several years with normal precipitation (average 484 mm in Table 2), rainfall was only 235 mm in 2001 and 286 mm in 2002. Low rainfall during the spring of 2002 (Fig. 2a) caused θ measured in the upper 0.15 m to decline from midway between field capacity and wilting point (Table 2) after thawing in early April to near wilting point by early July (Fig. 2b). The earlier declines in the models were caused by rapid evaporation from soil surface layers, especially those 0.1 m thick (A.6.7), before leafout on DOY 145. Declines in θ were underes-

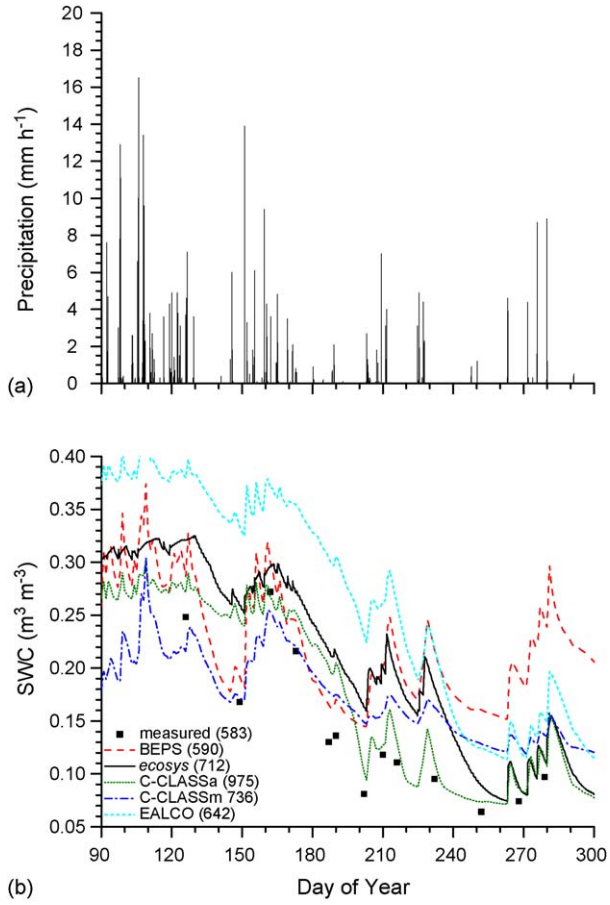

Fig. 1 – (a) Precipitation and (b) soil water contents (0–35 cm) measured (symbols) and modeled (lines) at Walker Branch during 1998. Numbers in parentheses represent total evapotranspiration (mm) calculated from gap-filled eddy covariance measurements (measured) or modeled during 1998.

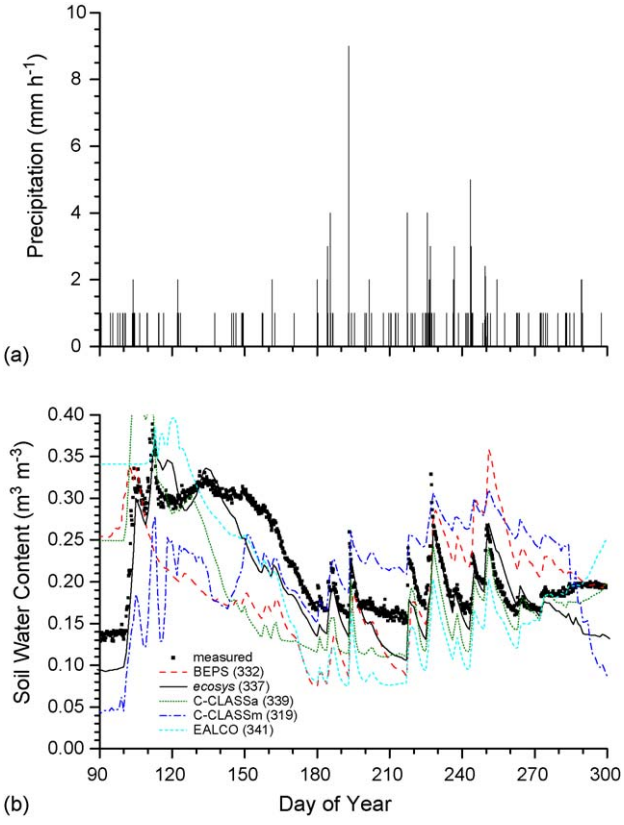

Fig. 2 – (a) Precipitation and (b) soil water contents (0–15 cm) measured (symbols) and modeled (lines) at Southern Old Aspen during 2002. Numbers in parentheses represent total evapotranspiration (mm) modeled during 2002.

timated by BEPS and C-CLASSm, as were those at WB (Fig. 1b), again likely because of differences in the allocation of water uptake among soil layers (A.6.6) because total ET was similar in all the models (Fig. 2b).

4.2. *Diurnal energy and CO_2 exchange during soil drying—measurement*

4.2.1. *Walker Branch*

Declining θ (Fig. 1b) caused soil water deficits to develop during early September 1998. CO_2 and energy exchange were examined during two comparable 3-day periods, the first before the onset of water deficits (DOY 214–216) and the second afterwards (DOY 256–258). During both periods, radiation reached 800 W m^{-2}, daytime T_a reached 30 °C (Fig. 3a), and daytime D reached 2 kPa (Fig. 3b). During the earlier period, most net radiation (R_n) was dissipated as latent heat (LE) and less as sensible heat (H), indicating that g_c did not much limit transpiration (Fig. 3c). During the later period, most R_n was dissipated as H rather than LE, indicating a strong stomatal limitation on transpiration.

Midday influxes of CO_2 were larger before the onset of water deficits than afterwards (~25 μmol m^{-2} s^{-1} versus ~15 μmol m^{-2} s^{-1} in Fig. 3d) in spite of comparable weather (Fig. 3a and b), indicating that soil water deficits were affecting canopy CO_2 fixation rates V_c. Influxes of CO_2 declined earlier during the day as water stress progressed. There was some scatter in the CO_2 fluxes, especially at night (e.g. DOY 215) when wind speeds were often <1 m s^{-1}, indicating that EC measurements were affected by low turbulence and had to be replaced by gap-filled values.

4.2.2. *Southern Old Aspen*

Declining θ (Fig. 2b) caused soil water deficits to develop by early July 2002. CO_2 and energy exchange were examined during two comparable 3-day periods, the first in late June before the onset of water deficits (DOY 172–174) and the second in late July after the onset of water deficits (DOY 204–206). During both periods, radiation exceeded 700 W m^{-2}, daytime T_a was 20–25 °C (Fig. 4a), and daytime D was 1.5–2.0 kPa (Fig. 4b). During the earlier period, R_n was dissipated about equally as LE and H (Fig. 4c) indicating that g_c only partially limited transpiration. During the later period, R_n was dissipated more as H than as LE, particularly on DOY 206 when radiation, T_a and D were high, indicating a greater stomatal limitation on transpiration.

Midday CO_2 influxes declined from 20 μmol m^{-2} s^{-1} before the onset of water deficits to 15 μmol m^{-2} s^{-1} afterwards

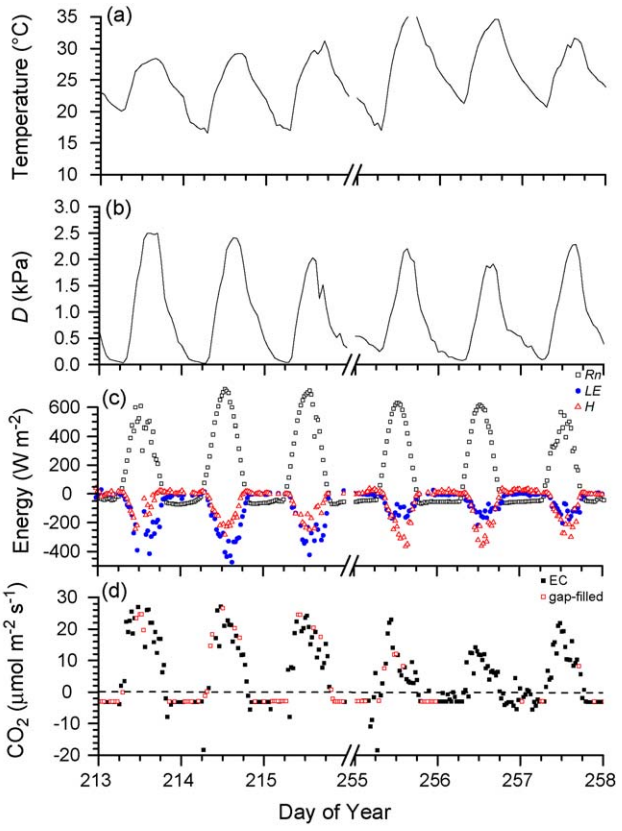

Fig. 3 – (a) Temperature, (b) vapor pressure deficit (*D*), (c) net radiation (R_n), latent heat (LE), sensible (*H*) heat and (d) CO_2 fluxes measured by eddy covariance (EC) (closed symbols) or gap-filled from EC measurements (open symbols) at Walker Branch during 2–4 August (DOY 214–216) and 13–15 September (DOY 256–258) 1998. Downward fluxes were assigned positive values, and upward fluxes negative values. Note decline in LE vs. *H* and earlier diurnal declines in CO_2 influxes in later vs. earlier period.

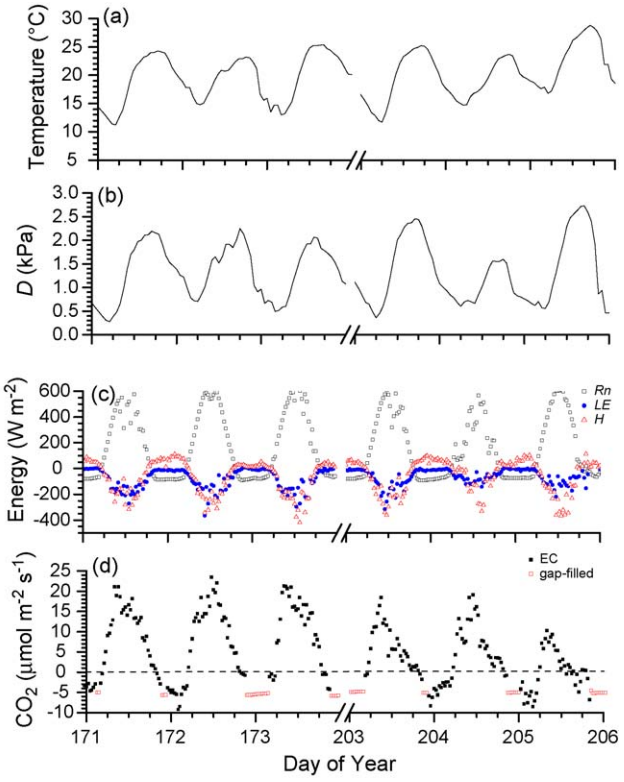

Fig. 4 – (a) Temperature, (b) vapor pressure deficit (*D*), (c) net radiation (R_n), latent heat (LE), sensible (*H*) heat and (d) CO_2 fluxes measured by eddy covariance (EC) (closed symbols) or gap-filled from EC measurements (open symbols) at Southern Old Aspen during 21–23 June (DOY 172–174) and 23–25 July (DOY 204–206) 2002. Downward fluxes were assigned positive values, and upward fluxes negative values. Note decline in LE vs. *H* and earlier diurnal declines in CO_2 influxes in later vs. earlier period.

(Fig. 4d) in spite of comparable weather (Fig. 4a and b), indicating that soil water deficits were affecting V_c. CO_2 influxes declined earlier during the day as water stress progressed, particularly on DOY 206 when radiation, T_a and *D* were high. Nighttime CO_2 effluxes did not appear to be much affected by soil water deficits.

4.3. *Diurnal energy exchange during soil drying—modeling*

4.3.1. *BEPS*

The transition from LE- to *H*-dominated energy exchange with declining θ at WB (Fig. 5a) was driven by declining ψ_s that forced lower g_l (A.2.1, A2.2) and hence LE (A.6.1). A tendency to underestimate LE and overestimate *H* under higher θ, due possibly to sensitivity of g_l to high T_a ($f(T)$ in A.2.1), may have slowed the modeled decline in θ, causing θ to be overestimated during September (Fig. 1b). The transition from LE- to *H*-dominated energy exchange with declining θ in the model was less apparent at SOA (Fig. 6a), where modeled θ did not decline during June and July (Fig. 2b). Afternoon advection of *H* sometimes modeled at both sites appeared to be caused by underestimation of afternoon R_n.

4.3.2. *Ecosys*

At WB, warm soil allowed rapid decomposition (A.5.11), mineralization (A.5.2) and uptake (A.3.3) of N that raised CO_2 fixation V_l (A.1.3, A.1.9). This rise, combined with that from higher T_c (A.1.2, A.1.8), increased g_l (A.2.1) so that rapid LE (A.6.1) was modeled under high radiation, T_a and θ during DOY 216–218 (Fig. 5b). Rapid LE caused rapid declines in θ (Fig. 1b) and ψ_s during August, which forced declines in ψ_c to maintain root water uptake (A.6.6). Declines in ψ_c caused declines in ψ_t and hence in g_l (A.2.2) that reduced LE and raised *H* during DOY 256–258, simulating the transition from LE- to *H*-dominated energy exchange (Fig. 5b). At SOA, high radiation, T_a and θ during DOY 172–174 allowed rapid V_l (A.1.2, A.1.8) and hence large g_l (A.2.1) and LE (A.6.1) that exceeded *H* (Fig. 6b), although measured fluxes did not. Declines in θ and ψ_s during July (Fig. 2b) forced declines in ψ_c to maintain root water uptake (A.6.6). Declines in ψ_c caused declines in ψ_t and hence g_l (A.2.2) that reduced LE and raised *H* during DOY 204–206 (Fig. 6b).

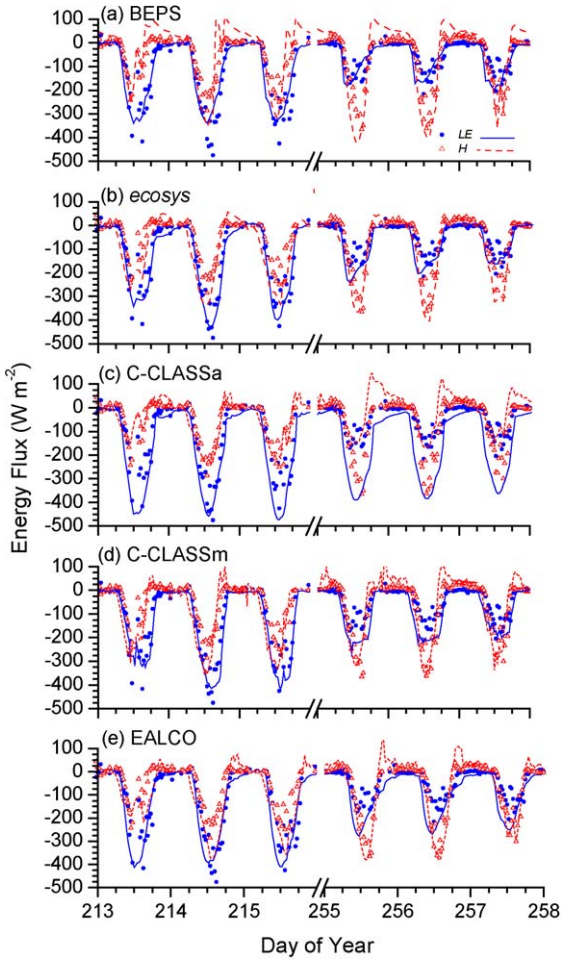

Fig. 5 – Latent (LE) and sensible (*H*) heat fluxes measured by eddy covariance (symbols) and modeled (lines) by (a) BEPS, (b) ecosys, (c) C-CLASSa, (d) C-CLASSm and (e) EALCO at Walker Branch during 2–4 August (DOY 214–216) and 13–15 September (DOY 256–258) 1998. Downward fluxes were assigned positive values, and upward fluxes negative values. Models simulated declines in LE vs. *H* to differing degrees in later vs. earlier period.

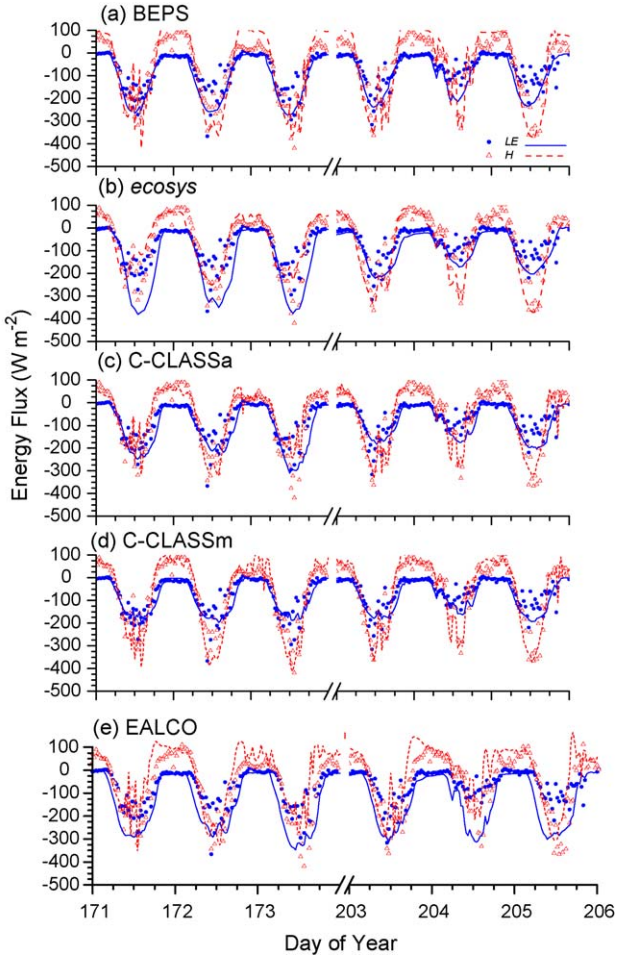

Fig. 6 – Latent (LE) and sensible (*H*) heat fluxes measured by eddy covariance (symbols) and modeled (lines) by (a) BEPS, (b) ecosys, (c) C-CLASSa, (d) C-CLASSm and (e) EALCO at Southern Old Aspen during 21–23 June (DOY 172–174) and 23–25 July (DOY 204–206) 2002. Downward fluxes were assigned positive values, and upward fluxes negative values. Slight declines in LE vs. *H* in the later vs. earlier period were simulated by most models.

4.3.3. *C-CLASSa*

Large V_{cmax} (A.1.1) caused large V_l (A.1.13) and hence large g_l (A.2.1) that caused overestimation of LE (A.6.1) and underestimation of *H* under higher θ at WB (Fig. 5c). Rapid LE caused rapid declines in near-surface θ to be accurately modeled during July and August (Fig. 1b). Declining ψ_s during September lowered ψ_c (A.6.6), V_l (A.1.4, A.1.10), g_l (A.2.1) and hence LE (A.6.1). However LE remained overestimated (Fig. 5c), likely because of excessive water uptake from deeper soil that contributed to large annual ET (Fig. 1b). LE was not overestimated before or during water deficits at SOA (Fig. 6c), although rapid early declines in θ caused depletion of water in the upper two soil layers before the first comparison period (Fig. 2b).

4.3.4. *C-CLASSm*

High radiation and T_a at WB in early August (Fig. 3a) before the onset of water deficits (Fig. 1b) caused rapid V_l (A.1.2, A.1.7), and hence large g_l (A.2.1) and LE (A.6.1) (Fig. 5d). Declining θ directly reduced V_l (A.1.4, A.1.10), and hence g_l (A.2.1, A.2.2) and LE (A.6.1) during September, but less than measured because the decline in θ from which modeled reductions in V_l and LE were calculated was smaller than that measured (Fig. 1b). LE and *H* modeled at SOA before water deficits in June were similar to those modeled during water deficits in July (Fig. 6d), because modeled near-surface θ rose from June to July, in contrast with measured values (Fig. 2b).

4.3.5. *EALCO*

Declines in θ (Fig. 1b) and ψ_s during September at WB forced declines in ψ_c to maintain root water uptake (A.6.6). Lower ψ_c caused lower V_l (A.1.4) and hence g_l (A.2.1), which in turn reduced LE and increased *H* (A.6.1) (Fig. 5e). LE in the model remained higher than that measured during September because θ was overestimated (Fig. 1b), likely because the effects of coarse fragments (Table 1) on θ were ignored.

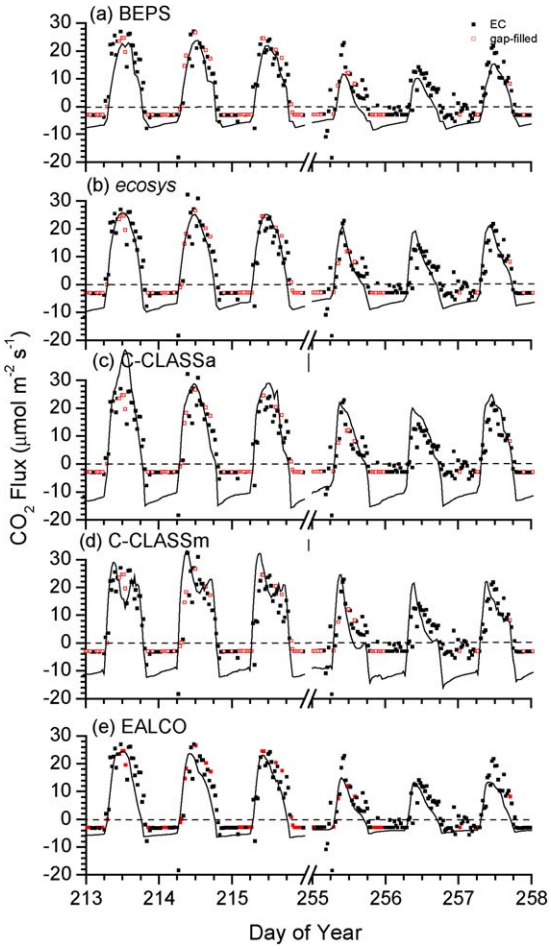

Fig. 7 – CO_2 exchange measured by eddy covariance (EC) (closed symbols) or gap-filled from EC measurements (open symbols) and modeled (lines) by (a) BEPS, (b) ecosys, (c) C-CLASSa, (d) C-CLASSm and (e) EALCO at Walker Branch during 2–4 August (DOY 214–216) and 13–15 September (DOY 256–258) 1998. Downward fluxes were assigned positive values, and upward fluxes negative values. Earlier diurnal declines in CO_2 influxes were simulated to differing degrees in the later vs. earlier period. Models that simulated larger CO_2 influxes also simulated larger CO_2 effluxes.

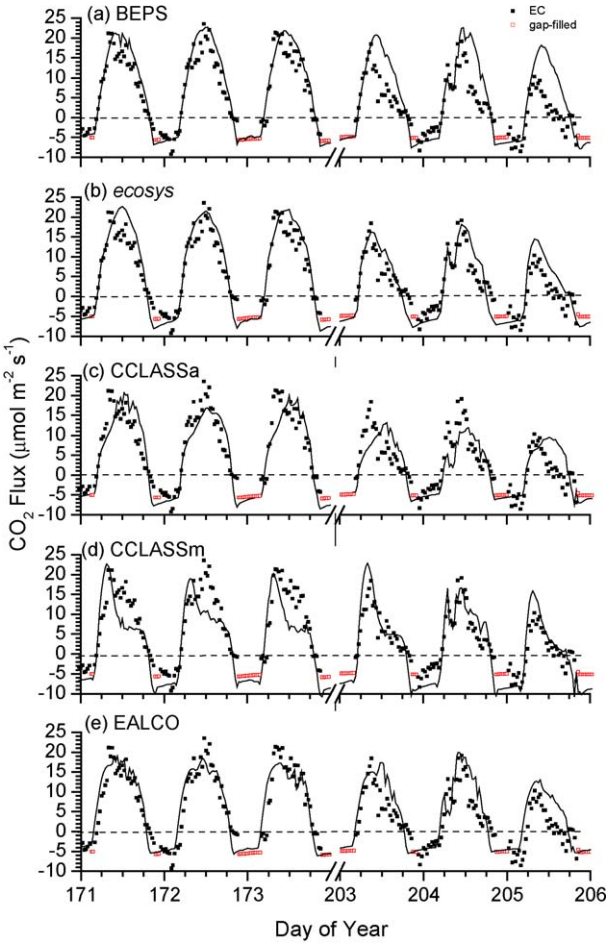

Fig. 8 – CO_2 exchange measured by eddy covariance (EC) (closed symbols) or gap-filled from EC measurements (open symbols) and modeled (lines) by (a) BEPS, (b) ecosys, (c) C-CLASSa, (d) C-CLASSm and (e) EALCO at Southern Old Aspen during 21–23 June (DOY 172–174) and 23–25 July (DOY 204–206) 2002. Downward fluxes were assigned positive values, and upward fluxes negative values. Only some of the models simulated earlier diurnal declines in CO_2 influxes in the later vs. earlier period.

However EALCO accurately captured the transition from LE-dominated to *H*-dominated energy exchange caused by soil drying at WB. LE at SOA tended to be overestimated, causing afternoon advection of *H* (Fig. 6e), even though θ was underestimated (Fig. 2b). There was little effect of soil drying during June and July on modeled LE even during DOY 206 when *D* was high (Fig. 4b), because ψ_c at SOA did not reach values to which V_l (A.1.4) and hence g_l (A.2.1) were sensitive.

4.4. *Diurnal CO_2 exchange during soil drying—modeling*

4.4.1. *BEPS*

CO_2 influxes declined with θ from August to September at WB (Fig. 7a) because lower ψ_s reduced g_l (A.2.1, A.2.2) and hence V_l (A.1.4). This reduction was particularly apparent during midafternoons because the effects of ψ_s on g_l were multiplied by those of *D*, and of T_a (A.2.1) which exceeded its optimum value for g_l of 25 °C during afternoons at WB (Fig. 3a). These multiplicative interactions may have caused declines in midafternoon CO_2 influxes to be slightly overestimated (e.g. DOY 256), given that the decline in near-surface θ was smaller than that measured (Fig. 1b). In general, the impact of soil drying on CO_2 and energy exchange was well captured by the model at WB. However at SOA CO_2 influxes declined little with soil drying from June to July (Fig. 8a) because modeled θ did not decline between the two comparison periods (Fig. 2b). Midday declines in CO_2 influxes measured during July under higher *D* (e.g. DOY 204 and 206) and lower θ were only partially simulated. Underestimation of these declines may possibly be attributed to the empirical g_l–*D* relationship of Dang et al. (1997) (A.2.1) which provided a weak response to the increase

in afternoon D. Also afternoon T_a during this period was close to optimum for g_l (A.2.1). CO_2 effluxes were in good agreement with measured and gap-filled values, indicating accurate R_a (A.4.1) + R_h (A.5.1) in the model.

4.4.2. *Ecosys*

Declining ψ_c during soil drying at WB and SOA imposed stomatal (A.2.2) and non-stomatal (A.1.4, A.1.10) constraints on V_l (A.1.13), which reduced CO_2 influxes (Figs. 7b and 8b). Diurnal declines in these influxes began earlier in the day when θ was lower, particularly under higher T_a and D (e.g. DOY 256 at WB and 206 at SOA). Earlier declines occurred because diurnal reductions in ψ_c became more rapid with declining ψ_s and rising soil and root axial resistances Ω_s and Ω_a (A.6.6), forcing earlier and larger reductions in g_l (A.2.2) and V_l (A.1.4, A.1.10). Lower V_l reduced plant non-structural C and hence R_a (A.4.1). At the same time, declining θ slowed decomposition (A.5.12), thereby slowing the production of DOC that drove R_h (A.5.1). Reductions in $R_a + R_h$ caused CO_2 effluxes to decline during water stress at WB (Fig. 7b) although these effluxes remained larger than those measured or gap-filled. Declines in R_h with soil drying during July at SOA (A.5.12) were offset by rises in R_h with soil warming (A.5.2), so that CO_2 effluxes changed little with θ (Fig. 8b).

4.4.3. *C-CLASSa*

Declining θ and ψ_s during September 1998 at WB (Fig. 1b) reduced ψ_c (A.6.6) and hence CO_2 influxes (A.1.4, A.1.10) (Fig. 7c). Diurnal reductions in CO_2 influxes began earlier with lower θ because declining ψ_c forced earlier declines in V_l (A.1.4, A.1.10). The large input value for V_{cmax} (A.1.1) caused CO_2 influxes to be overestimated during August at WB (Fig. 7c), lowering g_l (A.2.2) and causing LE effluxes to be similarly overestimated (Fig. 5c), accelerating soil drying (Fig. 1b). Lower ψ_s reduced R_h (A.5.12) and hence CO_2 effluxes, although modeled effluxes remained much larger than those measured or estimated by gap filling. Cooler T_a at SOA versus WB caused slower V_l, R_a and R_h (A.1.2, A.1.8, A.4.2, A.5.2), slower decomposition of litter and soil organic matter (A.5.11), hence slower N mineralization and uptake (A.3.3), and thus greater N constraints to V_l (A.1.3). Although sharp declines in θ (Fig. 2b) reduced CO_2 influxes, the model did not simulate the rapid midmorning influxes and earlier midday declines apparent during DOY 204–206 in the EC fluxes. Rising T_s during July caused CO_2 effluxes modeled during water deficits to decline little from those modeled earlier (Fig. 8c), as did measured and gap-filled effluxes.

4.4.4. *C-CLASSm*

Modeled CO_2 influxes showed sharp midday declines when θ was high at both WB (Fig. 7d) and SOA (Fig. 8d). These declines appeared larger than those measured, and were not apparent in modeled LE (Figs. 5d and 6d), suggesting that the combined non-stomatal (A.1.4, A.1.10) and stomatal (A.2.2) effects of θ on V_l (A.1.13) may have been overestimated under higher θ. The sharp midday declines in CO_2 influxes under higher θ at SOA may be attributed to the low value of D_0 (1.5 kPa) used to model D effects on g_l at this site (A.2.1). Midday declines in CO_2 influxes modeled under lower θ were more consistent with those in measured values (Figs. 7d and 8d). CO_2 effluxes were large in both August and September at WB (Fig. 7d) and rose from June to July at SOA (Fig. 8d), indicating limited sensitivity of $R_a + R_h$ (A.5.3) to declining θ. Large CO_2 effluxes in C-CLASSm were attributed to its large rate constant (A.5.1) and temperature sensitivity (A.5.2) for R_h of its single SOC pool.

4.4.5. *EALCO*

Soil drying caused peak CO_2 influxes to became smaller and diurnal reductions in CO_2 influxes to begin earlier at WB (Fig. 7e) and SOA (Fig. 8e) through the same processes as those described for ecosys and C-CLASSa that also used a ψ gradient approach to simulating θ effects on CO_2 and energy exchange (A.6.6). Lower CO_2 influxes on DOY 206 at SOA (Fig. 8e) were caused by low humidity (Fig. 4b) that lowered g_l (A.2.1), C_i and V_l (A.1.13). CO_2 effluxes at WB were smaller than those in other models (Fig. 7e), but declined well with θ (A.5.3). These low effluxes were attributed to low rate constants used for soil and litter C decomposition (A.5.9, A.5.10) combined with the low soil C content at WB (Table 1). CO_2 effluxes at SOA, where soil C content was larger (Table 2), were consistent with measured and gap-filled values, all of which changed little with θ (Fig. 8e).

4.5. *Diurnal CO_2 exchange during soil drying—measured versus modeled values*

4.5.1. *Walker Branch*

Modeled CO_2 fluxes screened for low u^* (0.175 m s^{-1} at WB and 0.2 m s^{-1} at SOA, see Section 4.8.2 below) were compared with measured values from DOY 210 to 229 inclusive when θ (0–35 cm) > wilting point (WP) and H < LE, and also from DOY 250 to 269 inclusive when θ < WP and H > LE. The response of measured fluxes to irradiance was clearly reduced during the later period when θ < WP (Fig. 9a), although T_a and D were comparable to those when θ > WP (Fig. 3a and b). BEPS tended to underestimate CO_2 influxes when θ > WP although it accurately simulated those when θ < WP (Figs. 7a and 9b), causing slopes from the regression of modeled on measured fluxes to rise from 0.9 to 1.0 with soil drying (b in Table 3). Negative intercepts from these regressions (a in Table 3) were caused by larger modeled versus measured nighttime effluxes (Fig. 7). Ecosys gave similar b values of ~1.1 when θ> or <WP (Table 3a), indicating that the average magnitude of θ effects on CO_2 fluxes was accurately simulated (Fig. 7b). However rapid early morning rises and midafternoon declines in CO_2 influxes modeled when θ < WP (Fig. 7b) caused a pronounced diurnal hysteresis in these fluxes that was not as apparent in the measured fluxes (Fig. 9c), raising RMSD (Table 3a). Large b and negative a from C-CLASSa (Table 3a) were caused by greater modeled versus measured influxes and effluxes of CO_2 (Figs. 7c and 9d). The large scatter of CO_2 fluxes in C-CLASSm, especially when θ < WP (Fig. 9e), was attributed to strong stomatal and non-stomatal effects of θ and D on CO_2 fixation, and to rapid CO_2 effluxes from drying soil (Fig. 7d), which raised b and RMSD, and lowered a (Table 3a). EALCO underestimated CO_2 fluxes similarly when θ> or <WP (Figs. 7e and 9f), so that b remained ca. 0.9 in both cases (Table 3a), indicating that the relative magnitude of θ effects on CO_2 exchange was accurately simulated.

Table 3 – Statistics from regression of simulated on observed hourly-averaged net CO_2 exchange at (a) Walker Branch (WB) during DOY 210–229 when θ (0–35 cm) > wilting point (WP) and during DOY 250–269 when θ < WP in 1998 and (b) Southern Old Aspen (SOA) during DOY 170–174 and DOY 182–186 when θ (0–15 cm) > WP, and during DOY 191–193 and DOY 204–210 when θ < WP in 2002

	BEPS	Ecosys	C-CLASSa	C-CLASSm	EALCO
(a) WB					
θ > WP (n = 205)					
b[a]	0.89	1.08	1.46	1.13	0.88
a[a] (μmol m^{-2} s^{-1})	−3.5	−4.7	−7.5	−4.5	−3.3
R^2[b]	0.84	0.80	0.85	0.77	0.80
RMSD[b] (μmol m^{-2} s^{-1})	4.4	4.9	4.2	5.3	4.9
θ < WP (n = 219)					
b	0.99	1.13	1.65	1.38	0.88
a (μmol m^{-2} s^{-1})	−3.4	−2.6	−5.2	−5.3	−1.6
R^2	0.76	0.68	0.77	0.67	0.71
RMSD (μmol m^{-2} s^{-1})	3.5	4.0	3.4	4.1	3.9
(b) SOA					
θ > WP (n = 191)					
b	0.98	1.01	0.84	0.90	0.91
a (μmol m^{-2} s^{-1})	1.8	0.2	1.0	0.6	1.0
R^2	0.89	0.86	0.71	0.68	0.90
RMSD (μmol m^{-2} s^{-1})	3.1	3.5	5.0	5.2	3.0
θ < WP (n = 193)					
b	1.10	1.00	0.70	1.14	0.95
a (μmol m^{-2} s^{-1})	2.9	1.0	1.2	−0.2	1.4
R^2	0.79	0.81	0.47	0.81	0.79
RMSD (μmol m^{-2} s^{-1})	3.5	3.3	5.5	3.3	3.4

[a] a, b from $Y = a + bX$, where Y is the modeled flux and X is the measured flux.
[b] R^2, RMSE from $Y = a + bX$, where Y is the measured flux and X is the modeled flux.

4.5.2. *Southern Old Aspen*

Modeled CO_2 fluxes were compared with measured values from DOY 170 to 174 and 182 to 186 inclusive when θ (0–15 cm) > WP and $H \sim$LE, and from DOY 191 to 193 and 204 to 210 inclusive when θ < WP and H > LE in 2002. The response of measured CO_2 fluxes to radiation declined from the earlier to later periods (Fig. 10a), although T_a and D were comparable (Fig. 4a and b), indicating θ effect on CO_2 exchange. BEPS did not fully model this decline (Figs. 8a and 10b), causing b from the regression of modeled on measured fluxes to rise to 1.1 during soil drying (Table 3b). Ecosys gave b of 1.0 with small a when θ > WP or θ < WP (Table 3b), indicating accurate modeling of θ effects on CO_2 fluxes at this site (Figs. 8b and 10c). C-CLASSa did not capture diurnal changes in CO_2 fluxes, especially when θ < WP (Fig. 8c), causing low b and large RMSD (Table 3b). The strong stomatal and non-stomatal effects of θ and D on CO_2 fixation in C-CLASSm (Fig. 8d) caused CO_2 influxes to be underestimated when θ > WP (b = 0.9), but better simulated fluxes when θ < WP (b = 1.1) (Fig. 10e; Table 3b). EALCO simulated θ effects on CO_2 fluxes well (Figs. 8e and 10f), giving similar b (0.90–0.95) and comparatively low RMSD when θ > WP or θ < WP (Table 3b).

4.6. *Daily soil CO_2 effluxes during soil drying—measurement and modeling*

4.6.1. *Walker Branch*

Soil drying at WB (Fig. 1b) reduced CO_2 influxes (Fig. 3d), but the small number of nighttime tower measurements did not permit inferences about how drying affected CO_2 effluxes. Soil CO_2 effluxes were measured by EC at a height of 1.5 m, and by static chambers at the soil surface. Daily totals of these fluxes rose with soil warming during May to reach ca. 4 g C m^{-2} day^{-1} (EC) or ca. 6 g C m^{-2} day^{-1} (chambers) during June and July, then declined with soil drying to <2 g C m^{-2} day^{-1} in late August and early September, rose with rainfall in mid-September, and then declined with soil cooling after early October (Fig. 11a). Effluxes measured by EC were lower than those by chambers because of low turbulence and some daytime CO_2 uptake by sparse surface vegetation.

Modeled soil CO_2 effluxes differed greatly in magnitude and time course. Effluxes in BEPS rose only slightly from winter to summer, likely because the Q_{10} of the R_h temperature function declined as T_s rose (A.5.2). CO_2 effluxes then declined only slightly with soil drying (A.5.12) in September (Fig. 11a), likely because of limited near-surface soil drying in the model (Fig. 1b). Soil CO_2 effluxes in ecosys rose sharply in spring, then declined sharply during soil drying (A.5.12) in September, and then rose with rainfall in late September (Fig. 11a). The large rise of R_h with T_s in ecosys during spring was attributed to higher-order effects of T_s on R_h (A.5.1) that drove more rapid growth of active microbial biomass (M_a in A.5.7 from R_g in A.5.6), hence more rapid decomposition (A.5.8) and DOC production, that in turn drove more rapid R_h (A.5.1). Gaseous transport algorithms in ecosys caused soil effluxes to be suppressed briefly by soil wetting during heavy precipitation, and to rise briefly with soil drying immediately afterwards, causing short-term variability in daily values during precipitation events. CO_2 effluxes in C-CLASSa were extremely large until August (Fig. 7c), likely because of the large respiration coeffi-

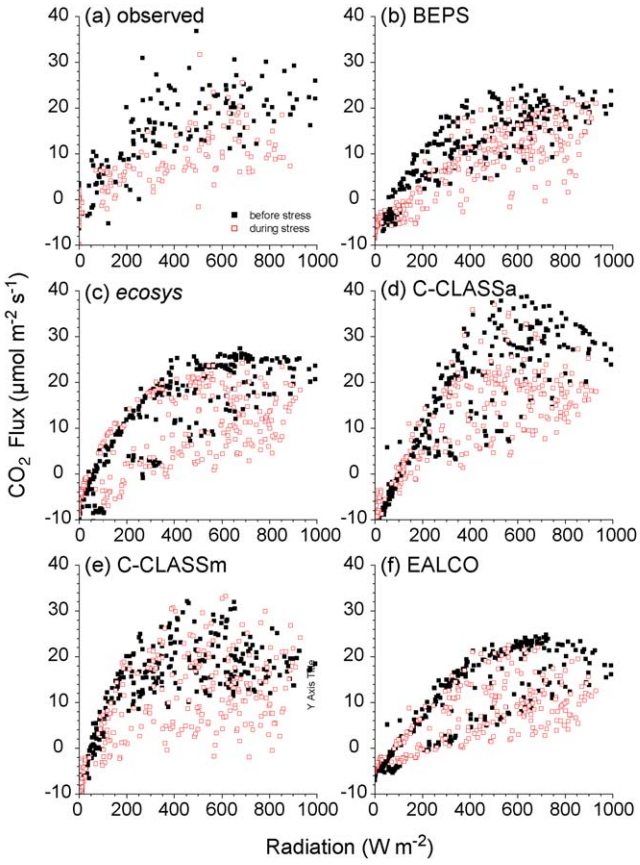

Fig. 9 – Response of CO_2 fluxes to radiation (a) measured and (b–f) modeled at Walker Branch during DOY 210–229 when θ (0–35 cm) > wilting point (WP) (closed symbols) and during DOY 250–269 when θ < WP (open symbols) in 1998.

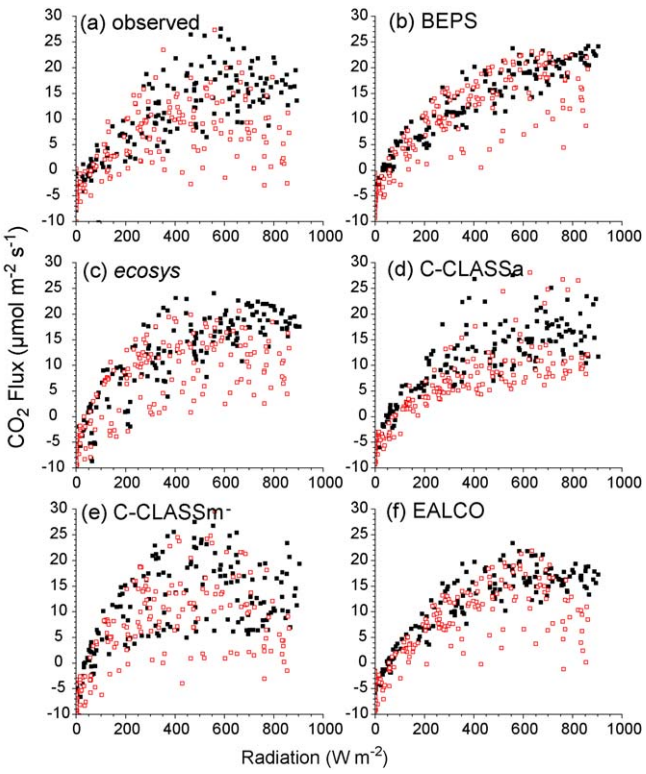

Fig. 10 – Response of CO_2 fluxes to radiation (a) measured and (b–f) modeled at Southern Old Aspen during DOY 170–174 and DOY 182–186 when θ (0–15 cm) > WP (closed symbols), and during DOY 191–193 and DOY 204–210 when θ < WP (open symbols) in 2002.

cients used for many of the SOC pools (A.5.1), then declined sharply with θ (A.5.12) in September (Figs. 1b and 11a). CO_2 effluxes in C-CLASSm rose during spring, but failed to decline with soil drying during August and September (Fig. 7d), likely because near-surface soil drying in the model was less than that measured (Fig. 1b), and because R_h of litter in C-CLASSm was not sensitive to θ (A.5.1, A.5.3). Soil CO_2 effluxes from EALCO were not provided.

4.6.2. *Southern Old Aspen*

Soil CO_2 effluxes were measured half-hourly by each of four automated surface chambers located about 50 m from the main EC tower. Daily totals of these effluxes rose with soil warming during May and June to reach 5–6 g C m^{-2} day^{-1} following a brief soil wetting in mid-July (Fig. 2b), after which effluxes declined with soil drying to 3 g C m^{-2} day^{-1} in early August (Fig. 11b). These declines were not apparent in the tower effluxes, many of which were gap-filled (Fig. 4d). Soil wetting in early August (Fig. 2a) caused a rapid return to higher effluxes until the end of the month, after which effluxes declined with soil cooling during September and October.

Variation among models in the magnitude and time course of soil CO_2 effluxes at SOA (Fig. 11b) was similar to that at WB (Fig. 11a). Effluxes in BEPS were larger than measured values in early spring and smaller in late spring and summer (Fig. 11b), partly because of low Q_{10} during soil warming (A.5.2), and partly because near-surface soil drying was modeled earlier in spring than was measured (Fig. 2b). These effluxes declined with further soil drying in July (A.5.12) and rose with soil wetting in August, but less than did measured values. Consequently, modeled effluxes remained below measured values even though ecosystem effluxes in the model agreed with those measured by EC (Fig. 8a). Effluxes in ecosys rose with measured values during warming in May and June, except during respiration of surface litter from the previous autumn modeled in mid-May, and then declined with measured values during drying (A.5.12; Fig. 2b) in July (Fig. 11b). Ecosys was unable to simulate the rapid rise in effluxes measured after rainfall events in mid-July and early August, even though rises in θ were accurately simulated (Fig. 2b). Therefore soil CO_2 effluxes measured under higher θ during July and August were underestimated even though ecosystem effluxes in the model agreed with EC measurements (Fig. 8b). As at WB, large effluxes from C-CLASSa during spring and early summer declined sharply with later soil drying (A.5.12). CO_2 effluxes in C-CLASSm were larger than those measured by EC during June and July (Fig. 8d) but were close to chamber measurements during most of the year (Fig. 11b). In contrast to those modeled at WB, CO_2 effluxes in C-CLASSm declined during soil drying at SOA (A.5.3), even though near-surface soil dry-

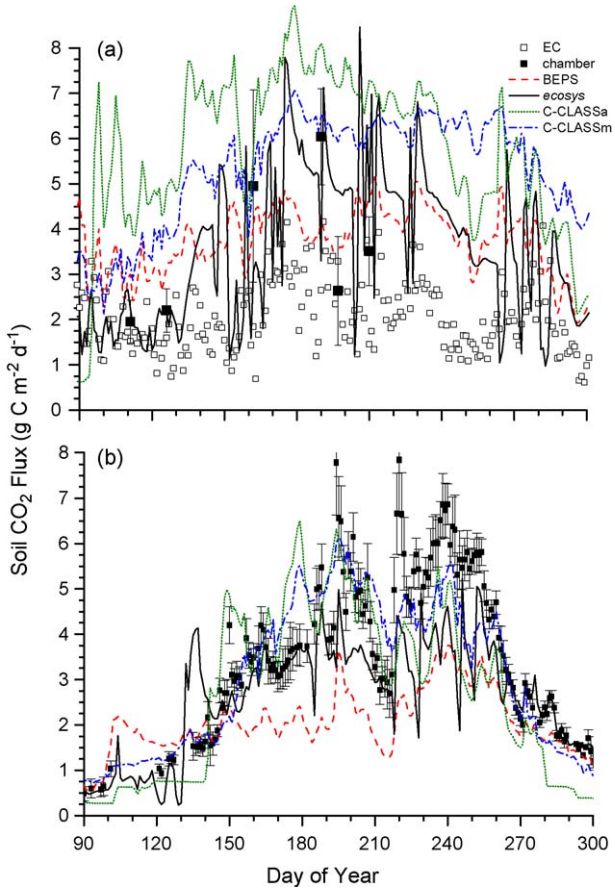

Fig. 11 – (a) Soil CO_2 fluxes measured by surface chambers (±S.E.) or by eddy covariance (EC) at 1.5 m above the soil surface (symbols), and modeled (lines) at Walker Branch during 1998, and (b) soil CO_2 fluxes measured by automated surface chambers (±S.E.) (symbols), and modeled (lines) at Southern Old Aspen during 2002. Models that simulated large CO_2 effluxes in Figs. 7 and 8 also simulated large soil CO_2 emissions.

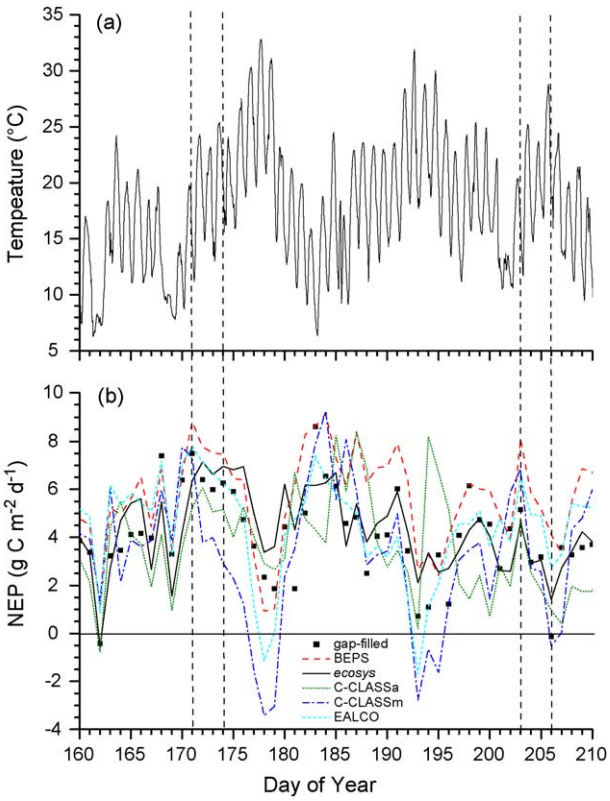

Fig. 12 – Net ecosystem productivity calculated from CO_2 fluxes measured by eddy covariance (EC) or gap-filled from EC measurements (symbols) and modeled (lines) at Southern Old Aspen during 2002. Vertical lines show flux comparison periods in Figs. 6 and 8. Measured declines in daily NEP in the later vs. earlier period were not fully captured by all models, especially under higher temperatures.

ing in the model was less than that measured (Fig. 2b). This decline may have been simulated because modeled θ at SOA was lower with respect to its values at field capacity and saturation (Table 2; A.5.3). Some of the divergence among declines in soil CO_2 effluxes modeled at both sites was attributed to different depth distributions of soil water uptake, leading to different θ during soil drying (Figs. 1b and 2b).

4.7. *Daily net ecosystem productivity during soil drying—measurement and modeling*

4.7.1. *Walker Branch*

Daily NEP was not calculated at WB because of the limited number of nighttime CO_2 flux measurements that were not replaced by gap-filled values during the period of interest (Fig. 3d).

4.7.2. *Southern Old Aspen*

Many nighttime CO_2 flux measurements were also replaced by gap-filled values at SOA (average of eight half-hourly values per day), but enough remained that calculated values of daily NEP were thought to be of interest. Soil drying at SOA (Fig. 2b) reduced CO_2 influxes (Figs. 4d and 10a) and effluxes (Fig. 11b), and so reduced NEP from 6–7 g C m^{-2} day^{-1} during June (DOY 171–175) to 0–3 g C m^{-2} day^{-1} during comparable weather in July (DOY 203–207) (Fig. 12). Reductions in NEP with soil drying were particularly apparent during warmer weather when sink activity declined sharply (DOY 192–196, DOY 206) due to midday declines in CO_2 influxes (Fig. 4d) and rises in CO_2 effluxes (Fig. 11b).

All models captured the direction of change in daily NEP during soil drying, although the magnitude of change varied among models as indicated from regressions of modeled versus measured NEP over the drying period (Table 4). BEPS captured much of the variation in NEP caused by changes in T_a during this period ($b = 0.80$, $R^2 = 0.57$ in Table 4), but overestimated NEP after DOY 180 when θ was low (Fig. 12; Table 3b) because midday declines in CO_2 influxes were not modeled (Fig. 8a) and soil CO_2 effluxes were underestimated (Fig. 11b). Midday declines in CO_2 influxes modeled by ecosys (Fig. 8b), were smaller than those measured under higher T_a (e.g. DOY 178–181, 193–196). Consequently, NEP declined with

Table 4 – Statistics from regressions of simulated on measured (b, a), and measured on simulated (R^2, RMSD), daily net ecosystem productivity (NEP) during a drying period (DOY 160–210) in summer 2002 at the Southern Old Aspen site

	BEPS	Ecosys	C-CLASSa	C-CLASSm	EALCO
NEP ($n=50$)					
b[a]	0.80	0.69	0.32	1.00	0.82
a (g m^{-2} day^{-1})	2.40	1.49	2.35	−0.80	1.03
R^2	0.57	0.60	0.08	0.43	0.54
RMSD (g m^{-2} day^{-1})	1.27	1.21	1.85	1.46	1.31

[a] $Y = a + bX$ from regression of simulated Y on measured X, R^2 and RMSD is the coefficient of determination and root mean square for difference from regression of measured Y on simulated X.

θ but less than was measured under higher T_a (Fig. 12), so that while modeled NEP was well correlated with measured values ($R^2 = 0.60$ in Table 4), it was positively biased ($b = 0.69$, $a = 1.49$ in Table 4). NEP in C-CLASSa responded well to soil drying, but was poorly correlated with measured NEP ($b = 0.32$, $R^2 = 0.08$ in Table 4; see also Table 3b) because modeled values rose sharply after rainfall events on DOY 185, 187 and 194 while measured values did not (Fig. 12). This divergence indicates the importance of correctly calculating root water uptake from soil layers with different θ caused by wetting and drying. In C-CLASSm, the large sensitivity of V_l to D and of R_h to T_s (Fig. 8d) caused modeled NEP to be more adversely affected by higher T_a than was measured NEP (Fig. 12), causing a negative bias ($a = -0.8$ g C m^{-2} day^{-1} in Table 4). However the effect of θ on NEP was well simulated ($b = 1.0$ in Table 4; see also Table 3b) because sharp declines in midday CO_2 influxes were modeled (Fig. 8d). NEP in EALCO responded comparatively well to changes in both T_a and θ ($b = 0.82$, $R^2 = 0.54$ in Table 4; see also Fig. 10f; Table 3b) because declines in midday CO_2 influxes were modeled (Fig. 8e). All models except C-CLASSm had a positive bias ($a > 0$ in Table 4), indicating a tendency to overestimate NEP.

4.8. *Hourly energy and CO_2 fluxes during the entire year—measured versus modeled*

4.8.1. *Energy fluxes at Walker Branch and Southern Old Aspen*

The partitioning of $R_n - G$ (soil + plant heat flux) into LE versus H indicated the degree of stomatal constraint imposed on forest CO_2 and energy exchange by water and nutrient limitations. Measurements of R_n were closely simulated by all models at both WB and SOA ($a \to 0$, $b \to 1$, $R^2 \to 1$ in Table 5) because measured shortwave, and in some cases longwave (C-CLASSa, C-CLASSm and EALCO), components of R_n were provided as model inputs. EC measurements of LE and H were screened for low u^* before comparison with modeled fluxes, but were not corrected for incomplete energy balance closure (yearly average 0.75–0.80 at WB (Wilson and Baldocchi, 2000) and 0.88 at SOA (Griffis et al., 2003)). Models that accurately partitioned $R_n - G$ into LE and H should therefore have had slopes from regressions of modeled on measured LE and H that were similar to each other, and slightly larger than one.

Based on these criteria, BEPS partitioned slightly less input energy into LE and slightly more into H than was measured at WB ($b = 0.89$ versus 1.29 for LE and H in Table 5a; also see Fig. 5a), causing lower ET and consequently less soil drying than was measured (Fig. 1b). This difference in partitioning was less apparent at SOA ($b = 1.07$ versus 1.31 for LE and H in Table 5b; see also Fig. 6a), indicating that g_l may have been underestimated under higher T_a at the warmer site ($f(T)$ in A.2.1). Conversely, C-CLASSa partitioned more energy into LE and less into H than was measured at WB ($b = 1.41$ versus 0.71 in Table 5a; Fig. 5c), and C-CLASSa and EALCO did so at SOA (Table 5b; Fig. 6e), causing rapid soil drying (Figs. 1b and 2b). This difference in partitioning was attributed to the large coefficient m used to calculate g_l in these two models (A.2.1). The partitioning of input energy by ecosys and C-CLASSm was more consistent with that measured at both sites ($0.9 < b < 1.2$ for LE and H in Table 4a and b).

The agreement between modeled and measured fluxes could be evaluated by comparing root mean squares for differences (RMSD) from regressions of measured on modeled fluxes with uncertainty in the measured fluxes. Baldocchi and Wilson (http://cdiac.esd.ornl.gov/ftp/ameriflux/data/us-sites/walker-branch/readme.wbw.flux) estimated the accuracy of the flux data recorded at Walker Branch to be ±4–7% for R_n, and the greater of ±15–20% or ±30 W m^{-2} for LE and H. Twine et al. (2000) estimated standard differences of LE measured by EC over a grassland to be between 17 and 48 W m^{-2}. Values for RMSD among the models of 39–45 W m^{-2} for LE and 40–52 W m^{-2} for H at WB (Table 5a) and of 23–30 W m^{-2} for LE and 43–57 W m^{-2} for H at SOA (Table 5b) were not likely to be significantly larger than standard errors of the measured fluxes. Scatter in the EC measurements therefore limited the confidence with which distinctions could be made among the accuracies with which the models in this study estimated LE and H.

4.8.2. *CO_2 fluxes at Walker Branch and Southern Old Aspen*

Measured CO_2 fluxes were screened for low u^* using the same criteria as those for LE and H. Measured CO_2 fluxes were not corrected for incomplete closure of the energy balance, although such correction has been estimated to raise gross CO_2 fixation and total ecosystem respiration estimated for boreal aspen by 10% (Griffis et al., 2003). Regressions of modeled on measured CO_2 fluxes (excluding gap-filled values) at WB indicated underestimation by BEPS ($b = 0.78$ in Table 5a; also see Table 3a; Fig. 7a), likely caused by the underestimation of g_l (A.2.1) and hence LE as noted earlier, and by EALCO

Table 5 – Statistics from regression of simulated on observed hourly-averaged net radiation (R_n), latent heat (LE), sensible heat (H) and net CO_2 exchange (CO_2) at (a) Walker Branch (WB) during 1998 and (b) Southern Old Aspen (SOA) during 2002

	BEPS	Ecosys	C-CLASSa	C-CLASSm	EALCO
(a) WB					
R_n (n = 8663)					
b[a]	1.00	1.04	1.02	1.04	1.10
a[a] ($W m^{-2}$)	−22	18	21	8	10
R^2[b]	0.87	0.97	0.97	0.97	0.97
RMSD[b] ($W m^{-2}$)	70	34	35	33	33
LE (n = 4946)					
b	0.89	1.10	1.41	1.10	1.17
a ($W m^{-2}$)	−8	−13	−20	−16	−2
R^2	0.71	0.78	0.77	0.68	0.76
RMSD ($W m^{-2}$)	43	37	38	45	39
H (n = 4687)					
b	1.29	1.27	0.71	0.91	1.20
a ($W m^{-2}$)	17	−20	−10	−12	−22
R^2	0.69	0.75	0.67	0.60	0.77
RMSD ($W m^{-2}$)	46	42	48	52	40
CO_2 (n = 2763)					
b	0.78	0.94	1.32	0.98	0.77
a ($\mu mol\ m^{-2}\ s^{-1}$)	−2.0	−1.4	−2.4	−0.3	0.9
R^2	0.71	0.70	0.73	0.58	0.70
RMSD ($\mu mol\ m^{-2}\ s^{-1}$)	4.4	4.5	4.2	5.3	4.5
(b) SOA					
R_n (n = 8463)					
b	1.11	0.96	0.93	0.93	1.02
a ($W m^{-2}$)	−23	11	8	5	0
R^2	0.97	0.96	0.99	0.99	0.99
RMSD ($W m^{-2}$)	31	33	17	12	21
LE (n = 6739)					
b	1.07	1.13	1.03	0.86	1.27
a ($W m^{-2}$)	−4	−2	−5	−9	1
R^2	0.76	0.73	0.70	0.60	0.77
RMSD ($W m^{-2}$)	24	25	26	30	23
H (n = 7305)					
b	1.31	0.99	0.73	0.72	0.96
a ($W m^{-2}$)	18	−16	−18	−17	−7
R^2	0.88	0.81	0.81	0.73	0.85
RMSD ($W m^{-2}$)	39	48	49	57	43
CO_2 (n = 5811)					
b	1.06	0.87	0.75	1.04	0.90
a ($\mu mol\ m^{-2}\ s^{-1}$)	0.2	0.1	0.2	0.4	0.1
R^2	0.87	0.81	0.73	0.81	0.88
RMSD ($\mu mol\ m^{-2}\ s^{-1}$)	2.0	2.5	2.9	2.5	2.0

[a] a, b from $Y = a + bX$, where Y is the modeled flux and X is the measured flux.
[b] R2, RMSE from $Y = a + bX$, where Y is the measured flux and X is the modeled flux.

(b = 0.77 in Table 5a; also see Table 3a; Fig. 7e), likely due to low V_{cmax} in A.1.1. These regressions also indicated overestimation by C-CLASSa (b = 1.32 in Table 5a; also see Table 3a; Figs. 7c and 11d), likely due to high V_{cmax} in A.1.1 (depending on leaf N content), which caused the overestimation g_l (A.2.1) and hence LE as noted earlier. Regression slopes for ecosys and C-CLASSm were close to one at WB (b = 0.94 and 0.98, respectively, in Table 5a; see also Table 3a).

Regressions of modeled on measured CO_2 fluxes at SOA indicated underestimation by C-CLASSa (b = 0.75 in Table 5b; see also Table 3b; Fig. 8c), attributed to lower leaf structural N:C ratios (A.1.1) caused by slower N mineralization (A.5.11) and uptake (A.3.3) from cooler soils. These model results indicate the additional complexities arising from the incorporation of a detailed N cycle in ecosystem models. Regressions for the other four models indicated closer agreement with EC fluxes at SOA (b = 1.06, 0.87, 1.04 and 0.90 for BEPS, ecosys, C-CLASSm and EALCO, respectively, Table 5b; see also Table 3b).

It is difficult to assess uncertainty in measured CO_2 fluxes when determining agreement between modeled and measured values. Twine et al. (2000) estimated that uncertainty in CO_2 flux measurements by EC over grassland varied between

10 and 30%. Values of RMSD for regressions of measured on modeled CO_2 fluxes ranged from 4.2 to 5.3 $\mu mol\,m^{-2}\,s^{-1}$ at WB (Table 5a) and from 2.0 to 2.9 $\mu mol\,m^{-2}\,s^{-1}$ at SOA (Table 5b). These values were comparable to average measured CO_2 fluxes of 5.8 and 3.2 $\mu mol\,m^{-2}\,s^{-1}$ measured at WB and SOA, respectively, indicating that better agreement between modeled and measured fluxes is needed for well-constrained model tests. Parameters from regressions of measured on modeled CO_2 fluxes were affected by measured nighttime effluxes that were frequently smaller than those modeled, especially at WB (e.g. DOY 256–258 in Fig. 7), causing negative intercepts ($a < 0$ in Table 5a). These parameters were also affected by large, scattered CO_2 influxes sometimes measured near midday that did not appear to be related to boundary conditions and so were not modeled (e.g. DOY 218 at WB in Fig. 7 and DOY 207 at SOA in Fig. 8).

4.9. *Annual ecosystem C balances*

Although the models in this study were comparable in the accuracy with which they could estimate measured CO_2 fluxes (Table 5a and b), modeled fluxes were achieved by a wide range of V_l (A.1.13) versus R_a (A.4.1) + R_h (A.5.1). C-CLASSm had the largest maximum rubisco-limited CO_2 fixation rate V_{rmax} (A.1.1) (that of C-CLASSa depended on leaf N content in A.1.3 and A.1.9), and EALCO had the smallest. These values were larger and smaller, respectively, than one of 60 $\mu mol\,m^{-2}\,s^{-1}$ measured for oak at WB by Wilson et al. (2001a,b) and used in BEPS. C-CLASSm and EALCO also gave the largest and smallest CO_2 influxes (Fig. 7c–e) and hence gross primary productivities ($GPP = \Sigma_t V_c = \Sigma_t \Sigma_l V_l$, where t is the time steps in a year and l is the leaf surfaces in a canopy) at both WB and SOA (Table 6a and b). Large GPP in C-CLASSm was also caused by a prescribed minimum LAI of 0.75 which caused GPP to be overestimated during the dormant season, and by a temperature function for V_l (A.1.2) that gave large values at lower temperatures.

Large GPP in C-CLASSm was offset by large R_m (from large rate constants for leaves and fine roots in A.4.3), and R_h (from large rate constants for different SOC and litter pools in A.5.9, A.5.10) that generated rapid CO_2 effluxes (Figs. 7d, 8d and 9a and b; Table 6a and b). These larger fluxes raised the sensitivity of daily NEP (=GPP − R_a − R_h) in C-CLASSm to soil and atmospheric water deficits (Fig. 12; Table 4). Small V_l from EALCO was offset by small R_a and R_h (Figs. 7e and 8e; Table 6a and b) so that NEP from C-CLASSm and EALCO differed less than did the component fluxes from which NEP was calculated. BEPS and ecosys gave intermediate GPP and $R_a + R_h$ at both sites (Table 6a and b), while C-CLASSa gave large GPP and $R_a + R_h$ at WB and small GPP and $R_a + R_h$ at SOA, which was consistent with the large and small regression parameters for CO_2 flux at WB and SOA (Table 6a and b). The impact of soil water deficits on NEP at SOA in 2002 was apparent from the much larger NEP measured and modeled in 2001 before the onset of drought (Table 6b).

Model values of GPP, R_a and R_h at WB and SOA could be constrained by biometric and micrometeorological estimates. Hanson et al. (2003a) estimated NPP (=GPP − R_a) at WB to be 638 $g\,C\,m^{-2}$ (Table 6a) but noted that the biometric measurements from which this estimate was derived could not account for changes in non-structural C stocks. Biometric measurements also could not account for rhizodeposition which can drive 20% of soil respiration in forest soils (Kelting et al., 1998), or about 0.2 × (R_h + below-ground R_a) ≈ 200 $g\,C\,m^{-2}$ at WB (cf. 174 $g\,C\,m^{-2}$ in ecosys). Given that annual changes in soil C at WB were considered to be small (gaining < 15 $g\,C\,m^{-2}\,year^{-1}$ according to Gaudinski and Trumbore, 2003), then an unaccounted C source of 180 $g\,C\,m^{-2}$ would be needed to offset the difference between R_h (559 $g\,C\,m^{-2}$) and litterfall (379 $g\,C\,m^{-2}$) calculated from measurements. This C source would raise NPP estimated by Hanson et al. (2003a) to 838 $g\,C\,m^{-2}$ which would bring it close to the 45:55 ratio with measured R_a (1189 $g\,C\,m^{-2}$) that has been found to be widely conserved in temperate forests (Waring and Running, 1998).

The above-ground R_a of 719 $g\,C\,m^{-2}$ calculated from chamber measurements at WB by Edwards and Hanson (2003) was smaller than those from C-CLASSa and C-CLASSm and larger than that from EALCO. An estimated GPP (=NPP + R_a) at WB of 1827–2027 $g\,C\,m^{-2}$ was consistent with GPP from BEPS and ecosys, but was smaller than GPP from C-CLASSa and C-CLASSm and larger than GPP from EALCO. Model variation in R_a offset that in GPP so that NPP of all models but C-CLASSm were within the range of likely values derived from biometric measurements. Modeled litterfall (A.4.8), especially below-ground, exceeded that measured, offsetting higher modeled NPP so that, except for BEPS, gains in wood C (=above-ground NPP − litterfall) were close to that measured. The below-ground $R_a + R_h$ of 1029 $g\,C\,m^{-2}$ measured by Hanson et al. (2003b) was also smaller than those from C-CLASSa and C-CLASSm (Fig. 11a) and larger than that from EALCO. Model variation in R_h further offset that in GPP and R_a when deriving modeled NEP. Nonetheless, there were large relative differences in simulated NEP from all five models which could not be well constrained by measurements because of the large difference in biometric versus EC estimates of NEP at WB. Wilson and Baldocchi (2001) estimated an annual NEP of 592 $g\,C\,m^{-2}$ from EC fluxes with gap filling from their model CANOAK, which had been extensively tested with leaf and soil CO_2 flux measurements at WB. This estimate was larger than NEP from all of the models except C-CLASSm because measured or gap-filled CO_2 effluxes were consistently smaller than all modeled effluxes (Fig. 7). The NEP of 79 $g\,C\,m^{-2}$ estimated by Hanson et al. (2003a) from biometric measurements in 1998 was much smaller than those from all of the models except BEPS. However a mean NEP of 187 ± 67 $g\,C\,m^{-2}$ estimated by Hanson et al. (2003a) at WB from biometric measurements over eight years including 1998 was closer to other modeled values.

In a mature, undisturbed forest, Δsoil C is likely to be small in comparison to litterfall, and should equal total litterfall − R_h + ΔDOC + ΔDIC (dissolved inorganic C) − (DOC + DIC) lost by runoff and leaching. Because only ecosys accounted for DOC (A.5.1) and DIC, there terms were omitted from Table 6. For the other models, Δsoil C should have equalled total litterfall − R_h. However in some models total litterfall − R_h was larger (EALCO) or smaller (C-CLASSm) than likely values for Δ soil C at both sites, indicating that R_h had not equilibrated with litterfall during model spin-up. Such equilibration needs to be achieved before future model tests of R_h.

Table 6 – Annual C balances estimated from site measurements and modeled at (a) Walker Branch (WB) during 1998 and (b) Southern Old Aspen (SOA) during 2002

	Estimated[a]	BEPS	Ecosys	C-CLASSa	C-CLASSm	EALCO
(a) WB ($g C m^{-2}$)						
GPP	1827	1857	2195	3002	3500	1660
R_a						
Above	719[b]		846	1422	1419	438
Below	470[c]		450	689	685	500
Total	1189	1308	1296	2111	2104	938
NPP	638	549	899	891	1396	722
Litter						
Above	251	310	268	403	295	266
Below	128	194	260	316	261	201
Exudation			174	56		
Total	379	504	702	775	556	722
ΔWood C	218	55	247	228	253	256
R_h	559[c]	448	591	652	782	351
Soil respiration	1029	1082	1041	1341	1467	851
Δsoil C			110	45	73	
NEP	79, 592[d]	101	308	239	614	371
LAI late June	6.0		5.4	6.8	6.2	
	Estimated	BEPS	Ecosys[e]	C-CLASSa	C-CLASSm	EALCO
(b) SOA ($g C m^{-2}$)						
GPP	1020	1274	1108	1046	1489	954
R_a						
Above			379	286	570	206
Below			275	260	311	332
Total		890	654	546	881	538
NPP		385	454	500	608	416
Litterfall						
Above		257	181	235	173	238
Below		118	139	210	130	87
Exudation			89	88		
Total		375	409	533	303	325
ΔWood C		10	107	106	115	92
R_h		204	353	365	426	262
Soil respiration			628	625	737	594
Δsoil C			66	23	91	
NEP	140	180	101	135	182	155
NEP 2001	382	333	276	162		319
LAI late June			5.4	5.5	5.6	

[a] Estimated values for WB from biometric measurements of Hanson et al. (2003a) except where otherwise indicated. GPP was estimated as NPP + R_a.
[b] Edwards and Hanson (2003).
[c] Below-ground R_a estimated as half of soil respiration, R_h estimated as half of soil respiration plus coarse woody debris respiration measured by Hanson et al. (2003b).
[d] From gap-filled EC measurements of Wilson and Baldocchi (2001).
[e] Plant components of C balance are the sums of those for aspen and hazelnut.

5. Discussion

5.1. *Limitations of eddy covariance measurements in evaluating model performances*

Much attention has been paid to uncertainty in EC measurements of mass and energy exchange. This uncertainty may be attributed to three causes:

(1) EC measurements are most accurate under turbulent, well-mixed conditions, but likely underestimate CO_2 and energy fluxes under the stable boundary layers that frequently develop during nighttimes. This underestimation is thought to be caused by air subsidence and advection which can be exacerbated by topographic variation as at WB, and may not be corrected by accounting for within-canopy CO_2 storage. Fluxes recorded under stable condi-

tions (defined here as $u^* < 0.175\,m\,s^{-1}$ at WB and $0.2\,m\,s^{-1}$ at SOA) were therefore excluded from comparison with modeled fluxes (Tables 3 and 5). These fluxes were replaced by gap-filled values (Figs. 7 and 8) for estimating daily and annual NEP (Fig. 12; Table 6), although replacement necessarily reduced the constraint of model testing. Gap-filled CO_2 effluxes were usually larger than the measured effluxes that they replaced, so that increasing the value of u^* used in gap-filling substantially reduced estimates of annual NEP at SOA (Griffis et al., 2003) and elsewhere.

(2) Incomplete recovery by EC of absorbed radiant energy ($R_n - G$) as dissipated heat (LE + H) has been proposed by Twine et al. (2000) and Wilson et al. (2002) to correspond with incomplete measurement of CO_2 fluxes. Recoveries of 0.75–0.80 at WB and 0.88 at SOA indicate that both LE and CO_2 fluxes may have been as much as 25 and 13% larger than those measured at WB and SOA, respectively. However the validity of correcting EC measurements for incomplete energy recovery is not universally accepted, and so this correction was not applied to the fluxes in this study.

(3) Uncertainty in the performance of EC instruments and gap-filling algorithms, which might be attributed to: (1) random error of the flux measurements due to the statistical nature of the turbulent transport process, (2) systematic error of the flux measurement due to differences in instrument gains, systematic biases due to signal attenuation, etc., and (3) systematic differences in the gap filling algorithm used to derive annual totals of NEP from an incomplete record of half-hourly EC measurements. The random error is commonly assumed to be less than 20% (Wesely and Hart, 1985), so that correlations between measured and modeled fluxes cannot be expected much to exceed 80%. Because of its random nature this error makes only a minor contribution to uncertainty of annual totals of NEP (Morgenstern et al., 2004a). To control the systematic error in the EC measurement intercomparisons between two independent EC systems were carried out at four sites of the FCRN with similar EC equipment, calibration procedures and maintenance standards to SOA (Morgenstern et al., 2004b). For all four sites turbulent fluxes of H, LE and CO_2 agreed to within 5%. Since this is a systematic difference between measurements, this uncertainty would also be present in that of the annual sum which has been estimated to be about 25% at SOA (Griffis et al., 2003), depending on the distribution of gaps over the year and the treatment of energy balance closure.

CO_2 effluxes from all models were consistently larger than those measured or gap-filled from EC measurements, especially at WB (Fig. 7). Consequently, modeled NEP was much lower than that estimated from EC measurements at WB. However they were higher than a biometric estimate at WB from the same year (Table 6a), and closer to a long-term mean biometric estimate. CO_2 effluxes in the models were driven from the products of CO_2 influxes, either directly through R_g (A.4.5), or indirectly through R_m of plant biomass (A.4.3) and R_h of plant litterfall (A.5.1). These effluxes were calculated using independent and established parameters for R_m (A.4.3), R_g (A.4.5) and R_h (A.5.1), so that their values in the models were well constrained with respect to V_l. Accurate modeling of CO_2 influxes measured under favorable conditions should therefore improve confidence in modeled CO_2 effluxes when measured values are not available. Modeled CO_2 effluxes may in future be used in place of gap-filled values when estimating annual NEP from EC measurements.

Each model forced energy balance closure when solving for energy exchange (A.6.1), so that all $R_n - G$ was recovered as LE + H. Because measured R_n was closely simulated, LE + H from most models exceeded that measured by amounts consistent with the LE + H not recovered by the EC measurements ($b > 1$ for LE and H in Table 5). However CO_2 fluxes from most models did not exceed those measured by corresponding amounts, indicating that correction of EC CO_2 fluxes for incomplete closure of the energy balance would have caused these fluxes to become larger than those modeled. This correction would have raised annual NEP estimated from EC fluxes (Griffis et al., 2003; Morgenstern et al., 2004a), so that these estimates, currently within the range of modeled NEP at SOA (Table 6b) and above it at WB (Table 6a), would have become larger than modeled values. Further model testing would benefit from greater certainty in measured CO_2 fluxes.

5.2. *Ability of different techniques to model CO_2 exchange during soil drying*

5.2.1. *Gross primary productivity*

Soil drying caused sharp reductions in sink activity for several weeks during the summers of 1998 at WB (Figs. 3d and 9a) and 2002 at SOA (Figs. 4d and 10a). The ability of the models in this study to simulate this reduction depended upon their ability to simulate midday declines in CO_2 influxes during soil drying, particularly under larger D, from the effects of declining ψ_s on V_l through stomatal and (optionally) non-stomatal processes. Wilson et al. (2001a,b) found that midafternoon declines in CO_2 and energy exchange measured during soil water deficits could not be modeled solely from the response of g_l to atmospheric humidity as earlier proposed by Collatz et al. (1991) and currently implemented in several ecosystem models. They suggested that modeling gas exchange during soil water deficits would require modeling hydraulic limitations in soils and plants.

The models in this study used different techniques to model these hydraulic limitations. One technique (ecosys, C-CLASSa and EALCO) was to solve for ψ_c at which water uptake from all rooted soil layers, determined by ψ_s and by Ω_s, Ω_r and Ω_a in each layer (A.6.6), equilibrated with transpiration, determined by radiation, T_a, D, wind speed and g_l through the canopy energy balance (A.6.1). The equilibrium ψ_c then constrained V_l (non-stomatal effect in A.1.4, A.1.10) and g_l (stomatal effect in A.2.1) so that V_c was affected by soil and atmospheric water deficits, and by soil and root hydraulic limitations. This technique does not yet account for a direct root-derived signal to moderate g_l.

Hydraulic limitations in these models changed with ψ_s, so that the sensitivity of g_l to D depended on ψ_c, ψ_r and hence ψ_s, thereby avoiding a fixed sensitivity of g_l to D that has been shown to be inconsistent with measurements (e.g. Wever et al., 2002). When ψ_s was high, Ω_s, Ω_r and Ω_a were

low, allowing ψ_c and ψ_t modeled under diurnal changes in D to remain at values to which g_l was insensitive (e.g. DOY 216–218 in Fig. 5b, c and e and DOY 172–174 in Fig. 6b, c and e). As ψ_s declined during soil drying, Ω_s, Ω_r and Ω_a increased, forcing ψ_c and ψ_t modeled under diurnal changes in D to decline to values to which g_l was sensitive (e.g. DOY 256–258 in Fig. 5b, c and e and DOY 204–206 in Fig. 6b, c and e). The rising sensitivity of g_l to D during soil drying allowed these models to simulate sustained rapid influxes of CO_2 on wet soil (e.g. DOY 216–218 in Fig. 7b, c and e and DOY 172–174 in Fig. 8b, c and e), as well as midday declines in CO_2 influxes on dry soil, starting earlier and becoming more rapid as soil drying progressed or as D rose (e.g. DOY 254 versus 256 in Fig. 7b and DOY 204 versus 206 in Fig. 8b). By calculating water uptake from ψ_c to ψ_s gradients in each soil layer (A.6.6), these models avoided assumptions used in other models to weight ψ_s or θ when calculating root water uptake from different soil layers. Avoiding these assumptions appeared to improve the simulation of near-surface θ by these models (Figs. 1b and 2b). However NEP in these models sometimes responded inappropriately to changes in θ (e.g. C-CLASSa in Fig. 12), likely because of low spatial resolution in the soil profile (A.6.7).

Another technique for modeling hydraulic limitations (BEPS) used an empirical non-linear relationship between ψ_s and g_l (A.2.2) to constrain V_l with no non-stomatal effect. This relationship between ψ_s and g_l was multiplied by that between D and g_l (A.2.1) so that g_l became more sensitive to ψ_s under higher D. The interaction between ψ_s and D on g_l enabled the simulation of earlier midday declines in CO_2 influxes at WB (Fig. 7a; Table 3a), but less so at SOA (Fig. 8a; Table 3b). However the accuracy of this approach in simulating seasonal and yearly mass and energy exchange could not be distinguished from that of hydraulic schemes by the EC data used in this study (Tables 3 and 4a and b).

Yet another technique for modeling hydraulic limitations (C-CLASSm) used θ to constrain V_l (non-stomatal effect in A.1.4) which then constrained g_l, but with a sensitivity to D that depended on θ (stomatal effect in A.2.1). This technique addressed concerns about the non-unique sensitivity of g_l to D, and was able to simulate rapid midday declines in CO_2 influxes during soil drying (Figs. 7d and 8d). However it also simulated these declines on wetter soil (e.g. DOY 216–218 in Fig. 7d and DOY 172–174 in Fig. 8d) when measured declines were not evident. This large sensitivity of g_l to D caused modeled NEP to be more adversely affected by rises in T_a than was measured NEP (Fig. 12). During transition to water stress, comparatively large changes in CO_2 flux were associated with comparatively small changes in near-surface θ, and with even smaller changes in deeper θ (Figs. 1b and 2b versus Figs. 3d and 4d). The sensitivity of V_l to θ indicates that responses of V_l and g_l to θ in these models should be more non-linear than that in A.1.4, with appropriate representation of how these responses are affected by changes in θ with depth.

5.2.2. *Soil respiration*

The ability of the models in this study to simulate the impact of soil drying on NEP also depended upon their ability to simulate reductions in soil CO_2 effluxes caused by the effects of declining ψ_s or θ on R_h and R_a. The declines in θ measured at WB (Fig. 1b) were larger than, and those at SOA (Fig. 2b) were similar to, declines in θ associated with 25–50% reductions in soil respiration measured by Lavigne et al. (2004) in a Balsam fir stand. Similar reductions in soil respiration were measured at both sites in this study (Fig. 11), suggesting that all models should have been able to simulate substantial declines in soil CO_2 effluxes during soil drying at both sites. Reductions in soil CO_2 effluxes comparable with those measured were modeled by C-CLASSa from an exponential function of ψ_s on decomposition (A.5.12). Comparable reductions were also simulated by ecosys from θ effects on heterotrophic activity (A.5.12), but recovery following rainfall appeared to be underestimated (Fig. 11a and b). Reductions in soil CO_2 effluxes somewhat smaller than those measured were modeled by BEPS from a second-order function of θ on decomposition (A.5.12). Reductions in soil CO_2 effluxes were not modeled by C-CLASSm during soil drying at WB (Fig. 11a) but were at SOA (Fig. 11b) from a non-linear function of θ on R_h of SOC excluding litter (A.5.3). The parameterization of this function needs to be more robust so that the effects of soil drying on CO_2 effluxes are modeled at all sites.

5.3. *Comparison with other modeling of eddy covariance measurements*

The performance of the ecosystem models in this study could be evaluated by comparison with those of more specialized models that have been adapted to site conditions. CANOAK is a detailed, multi-layer biosphere–atmosphere gas exchange model with a Lagrangian turbulent transfer scheme (Baldocchi and Harley, 1995; Baldocchi, 1997) that has been parameterized at WB from seasonal measures of soil respiration, LAI and maximum leaf CO_2 fixation rates (V_{lmax} and J_{max}). CANOAK reproduced 82% ($b = 1.09$) and 83% ($b = 1.14$) of the variances in hourly measurements of CO_2 and water vapor fluxes, respectively, when aggregated into 2-week bins at WB during 1997, a year with ample rainfall (Baldocchi and Wilson, 2001). Ecosys, which was parameterized independently of site measurements, reproduced 80% ($b = 0.97$) and 86% ($b = 1.17$) of the variances in hourly CO_2 and water vapor fluxes, respectively, when aggregated into 2-week bins at WB in 1998, a year when fluxes were affected by soil water deficits. Williams et al. (1996) developed SPA, a detailed, multi-layer biosphere–atmosphere gas exchange model parameterized from site measurements of LAI, total leaf N and root density. This model was able to reproduce 82% ($b = 1.05$) and 83% ($b = 0.85$) of the variances in daytime hourly measurements of CO_2 and water vapor fluxes, respectively, during 25 well-watered summer days at the Harvard Forest. This performance was only slightly better than that by the models in this study during the entire year at WB (Table 5a). These results indicate that the performances of comprehensive, general-purpose ecosystem models such as those in this study can approach those of specialized, site-specific models. These results also indicate that ~20% of variance in EC fluxes remains unexplained by models, even those with detailed mass and energy transfer schemes. This unexplained variation may be caused by short-term, convective heat and gas transfers that would require higher-order closure schemes to be modeled.

6. Conclusions—summary of model performances

6.1. Gross primary productivity

The accurate modeling of soil drying effects on NEP required the accurate simulation of V_l as affected by:

(a) V_{rmax} (A.1.1) and its non-hydrological constraints (A.1.2–A.1.3) used to calculate V_l (A.1.13) and thereby g_l (A.2.1) so that LE and hence rates of decline in θ were properly simulated (Figs. 1b and 2b). Values that were too large would cause rapid LE through A.2.1 (e.g. Fig. 5c), and would accelerate soil drying (Fig. 1b) and its effects on NEP. Conversely values that were too small would slow LE and hence soil drying and delay effects on NEP. Values used in C-CLASSa and C-CLASSm were likely too large as evidenced by large half-hourly CO_2 influxes (Fig. 7c and d) that led to annual GPP that was larger than could be inferred from biometric or EC measurements at WB (Table 6a). These large CO_2 influxes had to be offset by similarly large soil CO_2 effluxes (Fig. 11a) to arrive at an annual NEP that was consistent with estimates from gap-filled EC measurements.

(b) The allocation of root water uptake driven by LE among soil layers differing in water status and root density (A.6.6). Such allocation has received inadequate attention in many modeling programs, leading to arbitrary schemes with little theoretical justification. Allocation schemes based on water potential gradients constrained by soil and root hydraulic resistances (ecosys, C-CLASSa and EALCO) allowed better simulation of near-surface θ (Figs. 1b and 2b) than did schemes based on root fraction (BEPS) or depth (C-CLASSm).

(c) The midday declines in V_l induced by declining θ, especially under higher D (e.g. DOY 206 in Fig. 8) that caused substantial reduction in daily NEP (Fig. 12). These declines could be simulated consistently from hydraulic schemes of soil–plant–atmosphere water transport (from A.1.4, A.2.2, A.6.1, A.6.6 in ecosys) in which the sensitivity of g_l to ψ_l rose with declining ψ_s and ψ_r because of rising Ω_s and Ω_r (Fig. 8b). These declines could possibly also be simulated from a combined chemical-hydraulic scheme as proposed by Tardieu and Davies (1993) in which the sensitivity of g_l to ψ_r would rise with declining ψ_l. Hydraulic schemes could be avoided by modeling the interaction of ψ_s or θ directly on g_l (from A.2.1 in BEPS) or indirectly on g_l through V_l (from A.1.4 in C-CLASSm). Midday declines in V_l during soil drying could sometimes be simulated with these alternative approaches (Fig. 7a and d), but sometimes were not simulated (Fig. 8a), or simulated when not measured (Fig. 8d), because this interaction is highly non-linear and difficult to parameterize.

6.2. Soil respiration

The accurate modeling of soil drying effects on NEP also required the accurate simulation of R_h as affected by θ. However theory and algorithms for the effects of θ on R_h are much less developed than are those for the effects of soil and atmospheric water status on V_l. Models that used functions of θ to modify decomposition (BEPS in A.5.12) or respiration (C-CLASSm in A.5.3) sometimes underestimated soil drying effects on soil CO_2 effluxes (Fig. 11a), but sometimes simulated them well (Fig. 11b). The use of θ to account for soil drying effects on heterotrophic activity is well supported by studies of microbial ecology. However differences in model performances at the two sites indicate that these functions need to account for more soil-specific hydrologic properties than just total porosity. Models that used functions of ψ_s to modify decomposition (C-CLASSa in A.5.12) simulated larger soil drying effects on soil CO_2 effluxes (Fig. 11a and b), but without modeled results from EALCO this observation is confined to only one function. Values of ψ_s in these functions were derived from total porosity, field capacity and wilting point of each soil, and so are more soil-specific. Models that used a function of θ effects on heterotrophic activity (ecosys in A.5.12) simulated moderate soil drying effects on soil CO_2 effluxes at both sites. This function is not commonly used in ecosystem models.

Acknowledgements

The Fluxnet-Canada Research Network is funded by the Natural Sciences and Engineering Research Council of Canada (NSERC), the Canadian Foundation for Climate and Atmospheric Sciences (CFCAS), and the Biological Implications of CO_2 Policy in Canada (BIOCAP). Computational facilities for ecosys were provided by the Multimedia Advanced Computational Initiative (MACI) at the Universities of Alberta and Calgary.

REFERENCES

Amthor, J.S., Goulden, M.L., Munger, J.W., Wofsy, S.C., 1994. Testing a mechanistic model of forest-canopy mass and energy exchange using eddy correlation: carbon dioxide and ozone uptake by a mixed oak–maple stand. Aust. J. Plant Physiol. 21, 623–651.

Amthor, J.S., Chen, J.M., Clein, J., Frolking, S., Goulden, M.L., Grant, R.F., Kimball, J.S., King, A.W., McGuire, A.D., Nikolov, N.T., Potter, C.S., Wang, S., Wofsy, S.C., 2001. Boreal forest CO_2 exchange and evapotranspiration predicted by nine ecosystem process models: inter-model comparisons and relationships to field measurements. J. Geophys. Res. 106, 33,623–33,648.

Anderson, D., 1998. BOREAS TE-01 Soils Data over the SSA Tower Sites in Raster Format, available online at [http://www-eosdis.ornl.gov/] from the ORNL Distributed Active Archive Center, Oak Ridge National Laboratory, Oak Ridge, TN, USA.

Arain, M.A., Black, T.A., Barr, A.G., Jarvis, P.G., Massheder, J.M., Verseghy, D.L., Nesic, Z., 2002. Effects of seasonal and interannual climate variability on net ecosystem productivity of boreal deciduous and conifer forests. Can. J. For. Res. 32 (5), 878–891.

Baldocchi, D.D., 1997. Measuring and modeling carbon dioxide and water vapor exchange over a temperate broadleaf forest during the 1995 summer drought. Plant Cell Environ. 20, 1108–1122.

Baldocchi, D.D., Wilson, K.B., 2001. Modelling CO_2 and water vapour exchange of a temperate broadleaved forest on daily to decadal time scales. Ecol. Model. 142, 155–184.
Baldocchi, D., Falge, E., Wilson, K., 2001. A spectral analysis of biosphere–atmosphere trace gas flux densities and meteorological variables across hour to multi-year time scales. Agric. For. Meteorol. 107, 1–27.
Baldocchi, D.D., Harley, P.C., 1995. Scaling carbon dioxide and vapor exchange from leaf to canopy in a deciduous forest. II. Model testing and application. Plant Cell Environ. 18, 1157–1173.
Ball, J.T., 1988. An analysis of stomatal conductance. Ph.D. Thesis. Stanford University, Stanford, CA, 89 pp.
Ball, J.T., Woodrow, I.E., Berry, J.A., 1987. A model predicting stomatal conductance and its contribution to the control of photosynthesis under different environmental conditions. In: Biggens, J. (Ed.), Progress in Photosynthesis Research. Martinus Nijhoff Publishers, Dordrecht, pp. 221–224.
Barr, A.G., Griffis, T.J., Black, T.A., Lee, X., Staebler, R.M., Fuentes, J.D., Chen, Z., Morgenstern, K., 2002. Comparing the carbon budgets of boreal and temperate deciduous forest stands. Can. J. For. Res. 32, 813–822.
Blanken, P.D., Black, T.A., Neumann, H.H., Den Hartog, G., Yang, P.G., Nesic, Z., Lee, X., 2001. The seasonal water and energy exchange above and within a boreal aspen forest. J. Hydrol. 245, 118–136.
Black, T.A., Den Hartog, G., Neumann, H.H., Blanken, P.D., Yang, P.C., Russell, C., Nesic, Z., Lee, X., Chen, S.G., Staebler, R., Novak, M.D., 1996. Annual cycles of water vapour and carbon dioxide fluxes in and above a boreal aspen forest. Global Change Biol. 2, 219–229.
Bonan, G.B., 1991. A biophysical surface energy budget analysis of soil temperature in the boreal forests of interior Alaska. Water Resour. Res. 27 (5), 767–781.
Bunnell, F.L., Tait, D.E.N., Flanagan, P.W., van Cleve, K., 1977. Microbial respiration and substrate weight loss. I. A general model of the influence of abiotic variables. Soil Biol. Biochem. 9, 33–40.
Chen, J.M., Liu, J., Cihlar, J., Goulden, M.L., 1999. Daily canopy photosynthesis model through temporal and spatial scaling for remote sensing applications. Ecol. Model. 124, 99–119.
Chen, J.M., Chen, W., Liu, J., Cihlar, J., 2000b. Annual carbon balance of Canada's forests during 1895–1996. Global Biogeochem. Cycles 14, 839–850.
Chen, J.M., Ju, W., Cihlar, J., Price, D., Liu, J., Chen, W., Pan, J., Black, T.A., Barr, A., 2003. Spatial distribution of carbon sources and sinks in Canada's forests based on remote sensing. Tellus B 55 (2), 622–642.
Chen, W.J., Chen, J.M., Liu, J., Cihlar, J., 2000a. Approaches for reducing uncertainties in regional forest carbon balance. Global Biogeochem. Cycles 14, 827–838.
Churkina, G., Running, S.W., 1998. Contrasting climatic controls on the estimated productivity of global terrestrial biomes. Ecosystems 1, 206–215.
Collatz, G.J., Ball, J.T., Grivet, C., Berry, J.A., 1991. Physiological and environmental regulation of stomatal conductance, photosynthesis, and transpiration: a model that includes a laminar boundary layer. Agric. For. Meteorol. 54, 107–136.
Dang, Q.L., Margolis, H.A., Coyea, M.R., Sy, M., Collatz, G.J., 1997. Regulation of branch-level gas exchange of boreal trees: roles of shoot water potential and vapor pressure difference. Tree Physiol. 17, 521–535.
Edwards, N.T., Hanson, P.J., 2003. Aboveground autotrophic respiration. In: Hanson, P.J., Wullschleger, S.D. (Eds.), North American Temperate Deciduous Forest Responses to Changing Precipitation Regimes. Ecological Studies, vol. 166. Springer-Verlag, NY, pp. 48–66.
Falge, E., et al., 2001. Gap filling strategies for defensible annual sums of net ecosystem exchange. Agric. For. Meteorol. 107, 43–69.
Farquhar, G.D., von Caemmerer, S., Berry, J.A., 1980. A biochemical model of photosynthetic CO_2 assimilation in leaves of C_3 species. Planta 149, 78–90.
Gaudinski, J.B., Trumbore, S.E., 2003. Soil carbon turnover. In: Hanson, P.J., Wullschleger, S.D. (Eds.), North American Temperate Deciduous Forest Responses to Changing Precipitation Regimes. Ecological Studies, vol. 166. Springer-Verlag, NY, pp. 190–209.
Gollan, T., Passioura, J.B., Munns, R., 1986. Soil water status affects the stomatal conductance of fully turgid wheat and sunflower leaves. Aust. J. Plant Physiol. 13, 459–464.
Grant, R.F., 2001. A review of the Canadian ecosystem model ecosys. In: Shaffer, M. (Ed.), Modeling Carbon and Nitrogen Dynamics for Soil Management. CRC Press, Boca Raton, FL, pp. 175–264.
Grant, R.F., 2003. Modelling topographic effects on net ecosystem productivity of boreal black spruce forests. Tree Physiol. 24, 1–18.
Grant, R.F., Juma, N.G., Robertson, J.A., Izaurralde, R.C., McGill, W.B., 2001. Long term changes in soil C under different fertilizer, manure and rotation: testing the mathematical model ecosys with data from the Breton Plots. Soil Sci. Soc. Am. J. 65, 205–214.
Grant, R.F., Oechel, W.C., Ping, C., Kwon, H., 2003. Carbon balance of coastal arctic tundra under changing climate. Global Change Biol. 9, 16–36.
Grant, R.F., Arain, A., Arora, V., Barr, A., Black, T.A., Chen, J., Wang, S., Yuan, F., Zhang, Y., 2005. Modelling high temperature effects on CO_2 and energy exchange in temperate and boreal coniferous forests. Ecol. Model. 188, 217–252.
Griffis, T.J., Black, T.A., Morgenstern, K., Barr, A.G., Nesic, Z., Drewitt, G.B., Gaumont-Guay, D., McCaughey, J.H., 2003. Ecophysiological controls on the carbon balances of three southern boreal forests. Agric. For. Meteorol. 117, 53–71.
Grote, R., Suckow, F., Bellman, K., 1998. Modelling of carbon-, nitrogen- and water-balances in Scots pine stands. In: Hüttl, R.F., Bellman, K. (Eds.), Changes of Atmospheric Chemistry and Effect on Forest Ecosystems. Kluwer Academic Publishers, Dordrecht, Netherlands, pp. 251–281.
Hanson, P.J., Amthor, J.S., Wullschleger, S., Wilson, K., Grant, R., Hartley, A., Hui, E.D., Hunt Jr., R., Johnson, D.W., Kimball, J., King, A., Luo, Y., McNulty, S., Sun, G., Thornton, P.E., Wang, S., Williams, M., Cushmann, R.M., 2004. Carbon and water cycle simulations for an upland oak forest using 13 stand level models: intermodel comparisons and evaluations against independent measurements. Ecol. Monogr. 74, 443–489.
Hanson, P.J., Edwards, N.T., Tschaplinski, T.J., Wullschleger, S.D., Joslin, J.D., 2003a. Estimating the net primary and net ecosystem production of a southeastern upland Quercus forest from an 8-year biometric record. In: Hanson, P.J., Wullschleger, S.D. (Eds.), North American Temperate Deciduous Forest Responses to Changing Precipitation Regimes. Ecological Studies, vol. 166. Springer-Verlag, NY, pp. 378–395.
Hanson, P.J., O'Neill, E.G., Chambers, M.L.S., Roiggs, J.S., Joslin, J.D., Wolfe, M.H., 2003b. Soil respiration and litter decomposition. In: Hanson, P.J., Wullschleger, S.D. (Eds.), North American Temperate Deciduous Forest Responses to Changing Precipitation Regimes. Ecological Studies, vol. 166. Springer-Verlag, NY, pp. 163–189.
Humphreys, E.R., Black, T.A., Ethier, G.J., Drewitt, G.B., Spittlehouse, D.L., Jork, E.-M., Nesic, Z., Livingston, N.J., 2003. Annual and seasonal variability of sensible and latent

heat fluxes above a coastal Douglas-fir forest, British Columbia, Canada. Agric. For. Meteorol. 115, 109–125.
Hunt Jr., E.R., Lavigne, M.B., Franklin, S.E., 1999. Factors controlling the decline in net primary production with stand age for balsam fir in Newfoundland assessed using an ecosystem simulation model. Ecol. Model. 122, 151–164.
Jarvis, P.G., 1976. The interpretation of the variations in leaf water potential and stomatal conductance found in canopies in the field. Philos. Trans. R. Soc. Lond. Ser. B 273, 593–610.
Kelting, D.L., Burger, J.A., Edwards, G.S., 1998. Estimating root respiration, microbial respiration in the rhizosphere, and root-free soil respiration in forest soils. Soil Biol. Biochem. 30, 961–968.
Kimball, J.S., White, M.A., Running, S.W., 1997. BIOME-BGC simulations of stand hydrologic processes for BOREAS. J. Geophys. Res. 102, 29043–29051.
King, A.W., Post, W.M., Wullschleger, S.D., 1997. The potential response of terrestrial carbon storage to changes in climate and atmospheric CO_2. Clim. Change 35, 199–237.
Kothavala, Z., Arain, M.A., Black, T.A., Verseghy, D., 2005. Evaluating fluxes of energy, water vapour and carbon dioxide over common crops. Agric. For. Meteorol. 133, 89–108.
Kramer, K., et al., 2002. Evaluation of six process-based forest growth models using eddy-covariance measurements of CO_2 and H_2O fluxes at six forest sites in Europe. Global Change Biol. 8, 213–224.
Landsberg, J.J., Waring, R.H., 1997. A generalized model of forest productivity using simplified concepts of radiation-use efficiency, carbon balance and partitioning. For. Ecol. Manage. 95, 209–228.
Lavigne, M.B., Foster, R.J., Goodine, G., 2004. Seasonal and annual changes in soil respiration in relation to soil temperature, water potential and trenching. Tree Physiol. 24, 415–424.
Letts, M.G., Roulet, N.T., Comer, N.T., Skarupa, M.R., Verseghy, D.L., 2000. Parameterization of peatland hydraulic properties for the Canadian Land Surface Scheme. Atmosphere-Ocean 38 (1), 141–160.
Liu, J., Chen, J.M., Cihlar, J., Park, W., 1997. A process-based boreal ecosystems productivity simulator using remote sensing inputs. Remote Sens. Environ. 62, 158–175.
Monteith, J.L., 1965. Evaporation and environment. In: Fogg, G.E. (Ed.), The State and Movement of Water in Living Organisms. Symp. Soc. Expl. Biol. Academic Press, London, pp. 205–234.
Morgenstern, K., Black, T.A., Humphreys, E.R., Griffis, T.J., Drewitt, G.B., Cai, T., Nesic, Z., Spittlehouse, D.L., Livingstone, N.J., 2004a. Sensitivity and uncertainty in the carbon balance of a Pacific northwest Douglas fir forest during an El Niño/El Niña cycle. Agric. For. Meteorol. 123, 201–219.
Morgenstern, K., Nesic, Z., Black, T.A., 2004b. An intercomparison eddy-correlation system for the Fluxnet-Canada Research Network. In: 26th Conference on Agricultural and Forest Meteorology, American Meteorological Society, Vancouver, BC.
Nikolov, N.T., 1997. Mathematical modeling of seasonal biogeophysical interactions in forest ecosystems. Ph.D. Thesis. Colorado State Univ., Ft. Collins.
Orchard, V.V., Cook, F.J., 1983. Relationship between soil respiration and soil moisture. Soil Biol. Biochem. 15, 447–453.
Pastor, J., Post, W.M., 1988. Response of northern forests to CO_2-induced climate change. Nature 354, 55–58.
Peters, L.N., Grigal, D.F., Curlin, J.W., Selvidge, W.J., 1970. Walker Branch Watershed Project: chemical physical and morphological properties of the soils of Walker Branch Watershed. In: Oak Ridge National Laboratory Technical Manual, ORNL-TM-2968, pp. 32–33.
Potter, C.S., 1997. An ecosystem simulation model for methane production and emission from wetlands. Global Biogeochem. Cycles 11, 495–506.
Reichstein, M., Tenhunen, J.D., Roupsard, O., Ourcival, J.-M., Rambal, S., Miglietta, F., Peressotti, A., Pecchiari, M., Tirone, G., Valentini, R., 2002. Severe drought effects on ecosystem CO_2 and H_2O fluxes at three Mediterranean evergreen sites: revision of current hypotheses? Global Change Biol. 8, 99–1017.
Schulze, E.-D., 1993. Soil water deficits and atmospheric humidity as environmental signals. In: Smith, J.A.C., Griffiths, H. (Eds.), Water Deficits: Plant Responses from Cell to Community. BIOS Scientific Publishers Ltd., Oxford, UK, pp. 129–145.
Tardieu, F., Davies, W.J., 1993. Root–shoot communication and whole-plant regulation of water flux. In: Smith, J.A.C., Griffiths, H. (Eds.), Water Deficits: Plant Responses from Cell to Community. BIOS Scientific Publishers Ltd., Oxford, UK, pp. 147–162.
Tuzet, A., Perrier, A., Leuning, R., 2003. A coupled model of stomatal conductance, photosynthesis and transpiration. Plant Cell Environ. 26, 1087–1096.
Twine, T.E., Kustas, W.P., Norman, J.M., Cook, D.R., Houser, P.R., et al., 2000. Correcting eddy-covariance flux underestimates over a grassland. Agric. For. Meteorol. 103 (3), 279–300.
Verseghy, D.L., 2000. The Canadian Land Surface Scheme (CLASS): its history and future. Atmosphere-Ocean 38 (1), 1–13.
Wang, S.S., Grant, R.F., Verseghy, D.L., Black, T.A., 2001. Modelling plant carbon and nitrogen dynamics of a boreal aspen forest in CLASS—the Canadian Land Surface Scheme. Ecol. Model. 142, 135–155.
Wang, S.S., Grant, R.F., Verseghy, D.L., Black, T.A., 2002a. Modelling carbon dynamics of boreal forest ecosystems using the Canadian Land Surface Scheme. Clim. Change 55 (4), 451–477.
Wang, S.S., Grant, R.F., Verseghy, D.L., Black, T.A., 2002b. Modelling carbon-coupled energy and water dynamics of a boreal aspen forest in a general circulation model land surface scheme. Int. J. Clim. 22 (10), 1249–1265.
Wang, S., Chen, W., Cihlar, J., 2002c. New calculation methods of diurnal distribution of solar radiation and its interception by canopy over complex terrain. Ecol. Model. 155, 191–204.
Wang, Y.P., Leuning, R., 1998. A two-leaf model for canopy conductance, photosynthesis and available energy. I. Model description. Agric. For. Meteorol. 91, 89–111.
Wang, Y.P., Jarvis, P.G., 1990. Description and validation of an array model—MAESTRO. Agric. For. Meteorol. 51, 257–280.
Waring, R.H., Running, S.W., 1998. Forest Ecosystems: Analysis at Multiple Scales, second ed. Academic Press, San Diego, CA.
Wesely, M.L., Hart, R.L., 1985. Variability of short term eddy-correlation estimates of mass exchange. In: Hutchinson, B.A., Hicks, B.B. (Eds.), The Forest–Atmosphere Interaction. D. Reidel, Dordrecht, pp. 591–612.
Wever, L.A., Flanagan, L.B., Carlson, P.J., 2002. Seasonal and interannual variation in evapotranspiration, energy balance and surface conductance in northern temperate grassland. Agric. For. Meteorol. 112, 31–49.
Williams, M., Malhi, Y., Nobre, A.D., Rastetter, E.B., Grace, J., Pereira, M.G.P., 1998. Seasonal variation in net carbon exchange and evapotranspiration in a Brazilian rain forest: a modelling analysis. Plant Cell Environ. 21, 953–968.
Williams, M., Rastetter, E.B., Fernandes, D.N., Goulden, M.L., Wofsy, S.C., Shaver, G.R., Mellilo, J.M., Munger, J.W., Fan,

S.-M., Nadelhoffer, K.J., 1996. Modeling the soil–plant–atmosphere continuum in a Quercus-Acer stand at Harvard Forest: the regulation of stomatal conductance by light, nitrogen and soil/plant hydraulic properties. Plant Cell Environ. 19, 911–927.

Wilson, K.B., Hanson, P.J., Mulholland, P.J., Baldocchi, D.D., Wullschleger, S.D., 2001a. A comparison of methods for determining forest evapotranspiration and its components: sap-flow, soil water budget, eddy covariance and catchment water balance. Agric. For. Meteorol. 106, 153–168.

Wilson, K.B., Baldocchi, D.D., 2001. Comparing independent estimates of carbon dioxide exchange over 5 years at a deciduous forest in the southeastern United States. J. Geophys. Res. 106 (34), 167–234, 178.

Wilson, K.B., Baldocchi, D.D., 2000. Seasonal and interannual variability of energy fluxes over a broadleaf temperate deciduous forest. Agric. For. Meteorol. 100, 1–18.

Wilson, K.B., Baldocchi, D.D., Hanson, P.J., 2001b. Leaf age affects the seasonal pattern of photosynthetic capacity and net ecosystem exchange of carbon in a deciduous forest. Plant Cell Environ. 24, 571–583.

Wilson, K., Goldstein, A., Falge, E., Aubinet, M., Baldocchi, D., et al., 2002. Energy balance closure at FLUXNET sites. Agric. For. Meteorol. 113, 223–243.

Wullschleger, S.D., Gunderson, C.A., Tharp, L.M., West, D.C., 2003. Simulated patterns of forest succession and productivity as a consequence of altered precipitation. In: Hansen, P.J., Wullschleger, S.D. (Eds.), North American Temperate Deciduous Forest Responses to Changing Precipitation Regimes. Springer, NY, pp. 433–446.

Zhang, Y., Grant, R.F., Flanagan, L.B., Wang, S.S., Verseghy, D.L., 2004. Recent developments and testing of a carbon-coupled Canadian land surface scheme in a water-stressed northern temperate grassland. Ecol. Model. 181, 591–614.

Zierl, R., 2001. A water balance model to simulate drought in forested ecosystems and its application to the entire forested area in Switzerland. J. Hydrol. 242, 115–136.